JOURNAL OF GEOPHYSICAL RESEARCH, VOL. 98, NO. D8, PAGES 14,797–14,816, AUGUST 20, 1993

Simulation of Summertime Ozone over North America

DANIEL J. JACOB, JENNIFER A. LOGAN, ROSE M. YEVICH,
GERALDINE M. GARDNER, CLARISA M. SPIVAKOVSKY, STEVEN C. WOFSY,
J. WILLIAM MUNGER, SANFORD SILLMAN [1], MICHAEL J. PRATHER [2],
MICHAEL O. RODGERS [3], HAL WESTBERG [4], and PATRICK R. ZIMMERMAN [5]

Division of Applied Sciences and Department of Earth and Planetary Sciences, Harvard University, Cambridge, Massachusetts

The concentrations of O_3 and its precursors over North America are simulated for three summer months with a three-dimensional, continental-scale photochemical model using meteorological input from the Goddard Institute for Space Studies (GISS) general circulation model (GCM). The model has 4°x5° grid resolution and represents non linear chemistry in urban and industrial plumes with a subgrid nested scheme. Simulated median afternoon O_3 concentrations at rural U.S. sites are within 5 ppb of observations in most cases, except in the south central United States where concentrations are overpredicted by 15-20 ppb. The model captures successfully the development of regional high-O_3 episodes over the northeastern United States on the back side of weak, warm, stagnant anticyclones. Simulated concentrations of CO and nonmethane hydrocarbons are generally in good agreement with observations, concentrations of NO_x are underpredicted by 10-30%, and concentrations of peroxyacylnitrates (PANs) are overpredicted by a factor of 2 to 3. The overprediction of PANs is attributed to flaws in the photochemical mechanism, including excessive production from oxidation of isoprene, and may also reflect an underestimate of PANs deposition. Subgrid nonlinear chemistry as captured by the nested plumes scheme decreases the net O_3 production computed in the United States boundary layer by 8% on average.

1. INTRODUCTION

This paper is the first of two presenting a three-dimensional, continental-scale simulation of O_3 over North America for three summer months. Our objectives are to understand the factors regulating O_3 over the United States in summer and to determine the exports of O_3 and its precursors from the United States to the global atmosphere. We focus here on model description and evaluation. The objectives are addressed in the companion paper [*Jacob et al.*, this issue].

Several three-dimensional regional models for O_3 over the United States have been developed in the past decade [*Liu et al.*, 1984; *Chang et al.*, 1987; *Carmichael et al.*, 1991; *McKeen et al.*, 1991; *Roselle et al.*, 1991]. These models all use fine grid resolution (20-100 km). They are designed to simulate high-O_3 episodes occurring over spatial scales of a few hundred km and temporal scales of a few days. We needed a model that could be applied conveniently over continental and seasonal scales. The model is described in section 2 and evaluated with observations in section 3. Conclusions are in section 4.

[1] Department of Atmospheric, Oceanic and Space Sciences, University of Michigan, Ann Arbor.
[2] Department of Earth Sciences, University of California, Irvine.
[3] Department of Atmospheric Sciences, Georgia Institute of Technology, Atlanta.
[4] Department of Civil and Environmental Engineering, Washington State University, Pullman.
[5] National Center for Atmospheric Research, Boulder.

Paper number 93JD01223.
0148-0227/93/JD-01223$05.00

2. MODEL DESCRIPTION

Framework

The model domain is shown in Figure 1. The grid is 4° latitude x 5° longitude, with nine layers in the vertical defined by a sigma (terrain following) coordinate, replicating the grid of a general circulation model (GCM) developed at the Goddard Institute for Space Studies (GISS). A one-summer archive of data from the GISS GCM 2 [*Hansen et al.*, 1983] is used as input to the model (Table 1). The archive includes 4-hour averages of dynamical variables (winds, mixing depths, convective mass fluxes) and 5-day averages of other meteorological variables (temperature, humidity, cloud reflectivities).

Table 2 lists the chemical tracers transported in the model: odd oxygen (O_x), NO_x, peroxyacylnitrates (PANs), CO, a lumped hydrocarbon with lifetime of less than 1 day (HC1), and a lumped hydrocarbon with lifetime of a few days (HC2). These six tracers afford a good representation of O_3 photochemistry in current mechanisms [*Jacob et al.*, 1989]. Use of O_x as a tracer instead of O_3 allows to transport NO and NO_2 together; O_3 concentrations are retrieved from model output by assuming O_x-NO_x photochemical steady state in the daytime and NO-O_3 titration at night. Peroxy radical reactions modify the daytime steady state but the effect on O_3 concentrations is negligible.

Horizontal boundary conditions at the edges of Figure 1 are defined by observed background concentrations of tracers dependent on altitude, latitude, and month [*Logan*, 1985; *Rudolph et al.*, 1987; *Spivakovsky et al.*, 1990a]. Boundary conditions for O_3 in July are shown in Figure 2. The stratospheric boundary conditions have negligible effect on the model troposphere because cross-tropopause fluxes are small relative to horizontal fluxes across the lateral model boundaries in the troposphere. Background tropospheric O_3 in the model is thus determined by advection of the tropospheric boundary conditions.

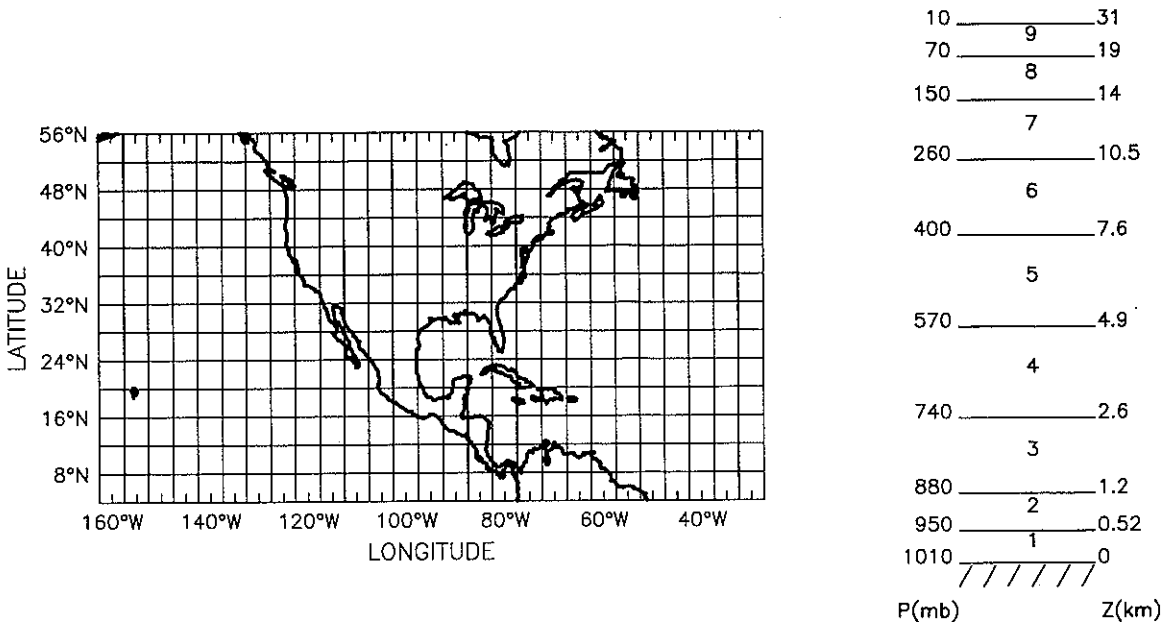

Fig. 1. Model domain and grid. The vertical grid (nine layers) is defined by a sigma coordinate; pressures and altitudes at layer boundaries are shown for an atmospheric column based at sea level.

The simulations are conducted from May 16 to August 31 of the GCM summer, starting from the boundary conditions. The period May 16-31 is used for initialization. Tracer concentrations $n(\mathbf{x},t)$ are updated over time steps Δt = 4 hours with a sequence of operators representing subgrid mass transfer from pollution plume boxes to rural air (S), transport across grid boxes (T), subgrid mass transfer into and between pollution plume boxes (S'), emissions (E), chemistry (C), and deposition (D):

$$n(\mathbf{x},t+\Delta t) = D.C.E.S'.T.S.n(\mathbf{x},t) \quad (1)$$

Concentrations of NO_x and HCl input to the C operator are partitioned into a fraction present at the beginning of the time step and a fraction released uniformly over the time step, to minimize the effect of operator splitting [*Jacob et al.*, 1989]. Tests presented by *Jacob et al.* [1989] show that the operator splitting procedure induces negligible error for O_3 and only small errors for NO_x and PANs (typically less than 20%). There is substantial error for HCl, which has a short lifetime, but this error has little effect on results for other tracers because the yields of O_3 and radicals per HCl molecule oxidized are properly represented.

Transport

Advection between grid boxes is computed with an upstream scheme conserving the second-order moments of tracer concentrations [*Prather*, 1986]. Dry and wet convective mass fluxes are computed as in the GCM [*Prather et al.*, 1987]. When an air column is unstable with respect to the dry adiabat (dry convection), the air within that column is mixed uniformly over the time step. When an air column is unstable with respect to the wet adiabat (wet convection), 50% of the air in the lowest layer is moved directly to the highest layer, with no entrainment, followed immediately by subsidence in the intermediate layers as necessary to conserve mass. Resolution of the mixed layer is limited by the coarse vertical grid (Figure 1). We have shown previously in a simulation of ^{222}Rn over North America that the model represents well the ventilation of the continental boundary layer [*Jacob and Prather*, 1990].

Chemistry

Rates of chemical production minus loss, *(P–L)*, are computed for each tracer with the detailed mechanism of *Lurmann et al.* [1986], modified as described by *Jacob et al.* [1989], and including the radiative transfer code of *Logan et al.* [1981]. For expedient computation, we parameterize the mechanism as

TABLE 1. GISS GCM Archive Used as Model Input

Variable	Temporal Resolution	Footnote
Surface pressure	4 hours	
Wind	4 hours	*a*
Mixing depth	4 hours	*b*
Convective events, total per column	4 hours	*c*
Convective events, vertical distribution	5 days	*c*
Solar radiation at surface	4 hours	
Cloud reflectivity (3 altitudes)	5 days	*d*
Temperature	5 days	*e*
Specific humidity	5 days	

GISS, Goddard Institute for Space Studies; GCM, general circulation model.

[a] Advective mass fluxes across grid box boundaries.

[b] Vertical extent of dry convective instability initiated by surface heating; archived as a fractional number of GCM layers [*Jacob and Prather*, 1990].

[c] The frequencies of dry, shallow wet, and deep wet convective events are archived separately. The dry convection frequencies do not include mixed layer convection, which is represented separately as the mixing depth. Shallow wet convection is defined as extending up to at most layer 3. The vertical distribution of convective events between pairs of layers within a column is computed at each 4-hour model time step by scaling the 5-day mean vertical distribution to the 4-hour totals of convective events in the column. The convective mass fluxes are computed from the frequencies of convective events as described by *Prather et al.* [1987].

[d] Cloud reflectivities at 800, 500, and 200 mbar, reconstructed to approximate the GCM vertical distribution of cloud optical depth [*Spivakovsky et al.*, 1990*a*].

[e] A sinusoidal diel cycle of temperature with amplitude 5 K and maximum at 15 LT (local time) is applied to the lowest model layer over land. Isoprene emission and surface resistances to deposition are computed using surface air temperatures, which are derived from the temperatures in the lowest model layer by assuming a dry adiabat.

TABLE 2. Chemical Tracers

Tracer	Composition
O_x	$O_3 + O + NO_2 + HNO_4 + (2x)NO_3 + (3x)N_2O_5$
NO_x	$NO + NO_2 + NO_3 + (2x)N_2O_5 + HNO_2 + HNO_4$
PANs	peroxyacetylnitrate (PAN) + higher peroxyacylnitrates
CO	
HC1	Hydrocarbons with lifetimes of less than a day
HC2	Hydrocarbons with lifetimes of a few days

Hydrocarbons lumped into HC1 include isoprene, > C_2 alkenes, xylenes, and other aromatics with ">2.0 reactivity" in the (NAPAP) inventory (i.e., aromatics oxidized by OH with rate constant $>1.3\times10^{-11}$ cm^3 molecule^{-1} s^{-1} at 298 K). Hydrocarbons lumped into HC2 include C_{3-11} alkanes, benzene, halobenzenes, toluene, ethylene, and other species with "0.25-2.0 reactivity" in the NAPAP inventory (i.e., species oxidized by OH with rate constant between 1.7×10^{-12} and 1.3×10^{-11} cm^3 molecule^{-1} s^{-1} at 298 K). The reactivity of HC1 is defined as that of isoprene in the continental boundary layer in daytime and as that of a 70/30 propene/isoprene mix under other conditions. The reactivity of HC2 is defined as that of a mix 13% propane, 32% $C_{4,5}$ alkanes, 20% C_{6-8} alkanes, 2% $C_{4,5}$ alkylnitrates, 6% C_{6-8} alkylnitrates, 8% benzene, 12% toluene, and 7% ethylene [*Jacob et al.*, 1989]. The partitioning of HC1 and HC2 is in units of atoms C.

polynomials of 11 independent variables defining the chemical environment (Table 3). The parameterization procedure is described by *Spivakovsky et al.* [1990*b*], and details are given in Appendix A. The polynomials in Table 3 include 4-hour average *(P–L)* for O_x, NO_x, and PANs and 4-hour average concentrations of OH and NO_3 from which *(P–L)* for CO, HC1, and HC2 are computed. Yields of CO from the oxidation of HC1, HC2, and methane (1.7 ppm) are taken as 60%, 30%, and 90%, respectively [*Lurmann et al.*, 1986]. The radiation field in the chemical parameterizations is defined by two photolysis rate constants, J_{NO_2} and $J_{O(^1D)}$, which are computed in turn as polynomials of seven independent variables parameterizing results from the radiative transfer code (Table 3). All independent variables in Table 3 are either computed in the model or specified by the GCM archive, except for the O_3 columns which are climatological means dependent on latitude and month [*Spivakovsky et al.*, 1990*a*].

Emissions

The model includes anthropogenic emissions of NO_x, CO, and non-methane hydrocarbons (NMHCs), and biogenic emission of isoprene, all released in the lowest model layer (Figure 3). North American anthropogenic emissions are taken from the summer 1985 inventory compiled by the National Acid Precipitation Assessment Program (NAPAP) [*Environmental Protection Agency (EPA)*, 1989]. The 24-hour average weekday NAPAP inventory defines the spatial distribution of emissions. Mean diel cycles are superimposed as given by the *EPA* [1989]. Emissions on Saturdays and Sundays are reduced from weekday values respectively by 14% and 22% for NO_x, 22% and 32% for CO, and 23% and 33% for NMHCs, based on averages from NAPAP. Emissions in Hawaii and Puerto Rico are scaled from the U.S. inventory on the basis of population. Anthropogenic emissions in Central and South America are estimated from national data for coal, oil, and gas consumption in 1980 [*United Nations*, 1984], combined with emission factors for each fuel, and are distributed spatially within each country on a per capita basis using a 1°x1° population map [*Logan et al.*, 1981; *Logan*, 1983; J. A. Logan, unpublished data, 1993].

Isoprene emission is a function of vegetation type, surface air temperature, and insolation (Appendix B). It is computed with 1°x1° resolution using the vegetation-type map of *Matthews* [1983] and is subsequently averaged over the 4°x5° grid. The maximum over the south central United States in Figure 3 reflects a combination of dense deciduous forest cover and high

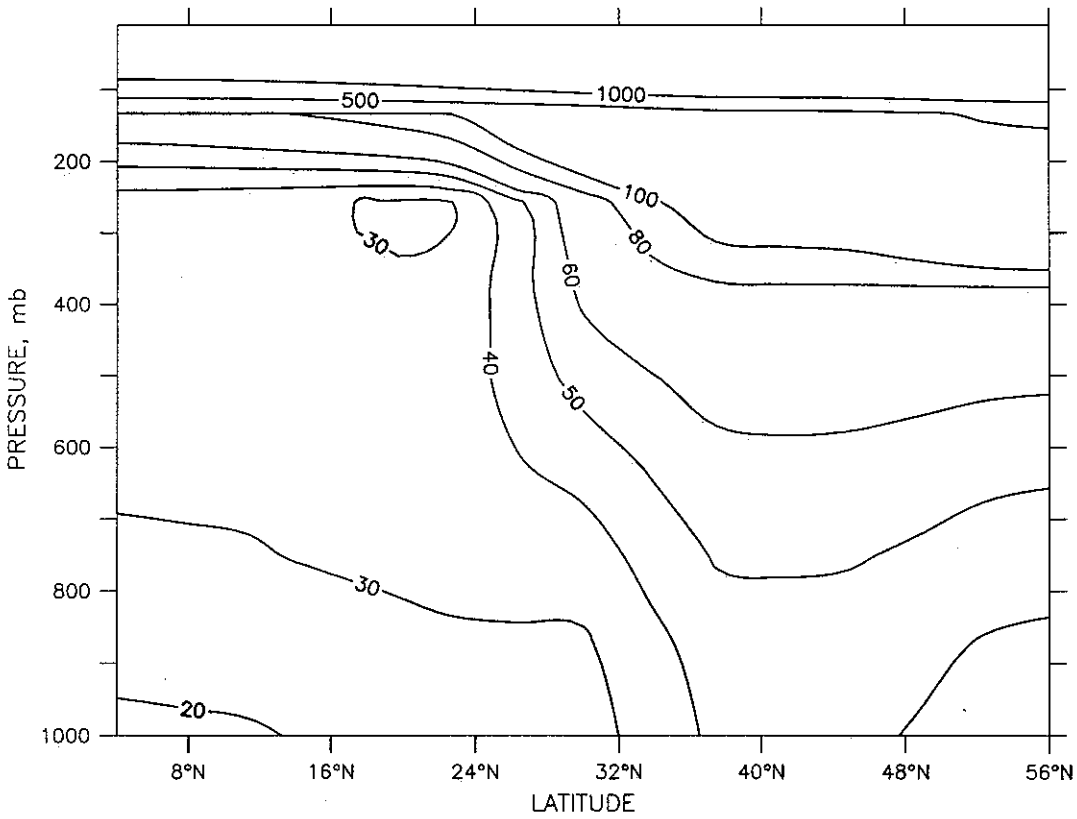

Fig. 2. Boundary conditions for O_3 (ppb) in July.

TABLE 3. Parameterized Polynomials in the Chemical and Radiative Computations

	Polynomial Output Variable	Independent Variables
Chemical		
	1. $(P-L)_{O_x}$	1. $[O_x]$
	2. $(P-L)_{NO_x}$	2. $[NO_x]$
	3. $(P-L)_{PANs}$	3. [PANs]
	4. [OH]	4. [CO]
	5. $[NO_3]$	5. [HC1]
		6. [HC2]
		7. $[H_2O]$
		8. Temperature
		9. Pressure
		10. J_{NO_2}
		11. $J_{O(^1D)}$
Radiative		
	1. J_{NO_2}	1. Solar zenith angle
	2. $J_{O(^1D)}$	2. Pressure
		3. O_3 column
		4. Surface albedo
		5. Cloud reflectivity at 800 mbar
		6. Cloud reflectivity at 500 mbar
		7. Cloud reflectivity at 200 mbar

$(P-L)_X$ is the net chemical production rate of X. J_{NO_2} and $J_{O(^1D)}$ are the rate constants for NO_2 photolysis and O_3 photolysis to $O(^1D)$, respectively.

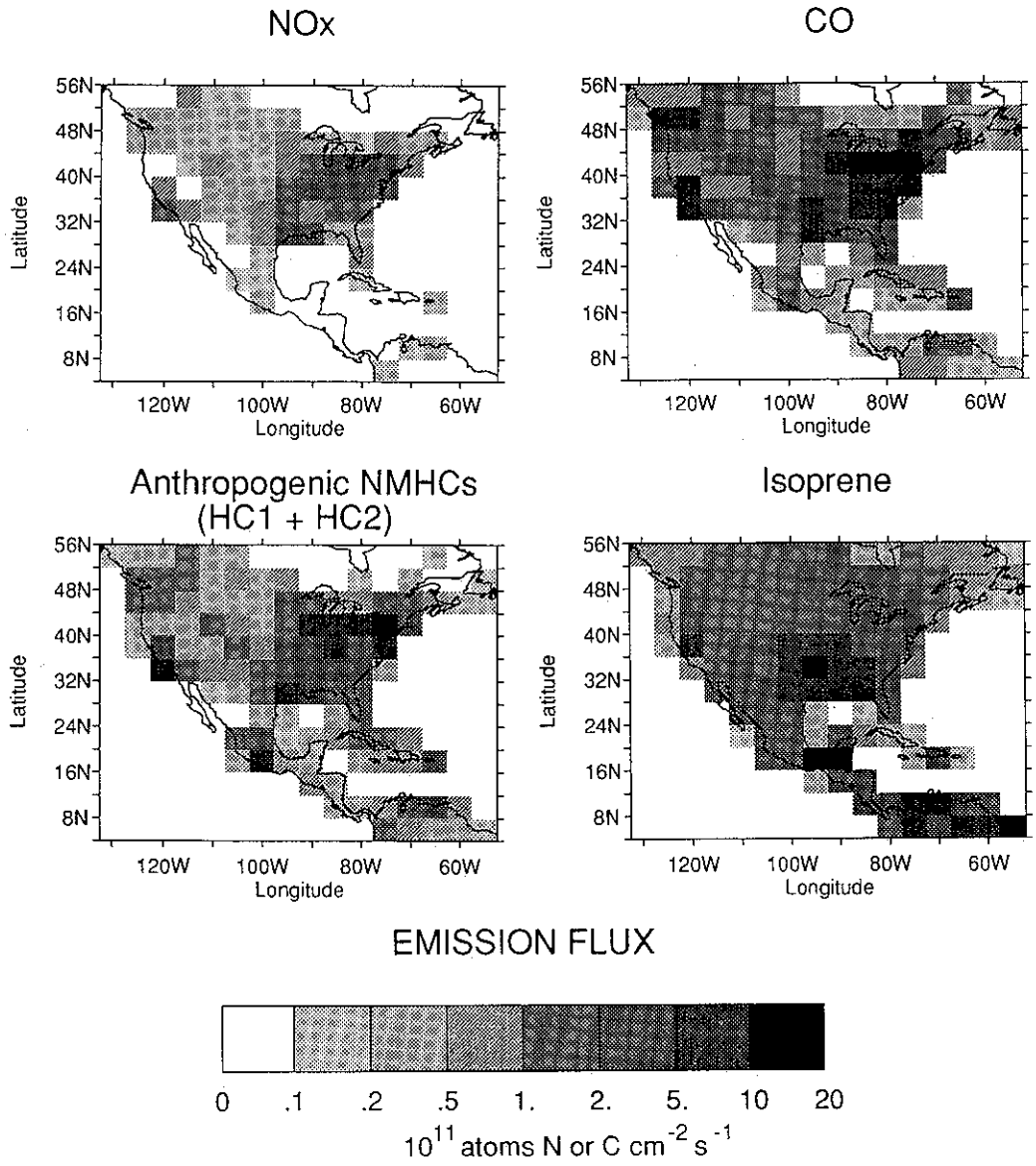

Fig. 3. Anthropogenic emissions of NO_x, CO, and nonmethane hydrocarbons (NMHCs) on a summer weekday, and biogenic emission of isoprene in July. Values are 24-hour averages.

temperatures. Isoprene is the principal contributor to HC1 emission everywhere except in cities.

Deposition

Deposition velocities of O_3, NO_x, and PANs are computed at the midpoint of the lowest layer (≈ 250 m above ground) using the resistance-in-series model of *Wesely and Hicks* [1977] with surface resistances and roughness heights from *Wesely* [1989], and surface-type information from *Matthews* [1983]. Friction velocities and Monin-Obukhov lengths are estimated with a Pasquill-Gifford parameterization dependent on wind speed, solar radiation flux, cloud cover, and roughness height [*Seinfeld*, 1986]. Under nighttime conditions over land the Monin-Obukhov length is generally less than 250 m, i.e., the atmosphere near the surface is strongly stratified, and we assume that deposition is negligible. Over water the atmosphere is assumed neutrally buoyant at all times, and the friction velocity is calculated from the local wind speed and roughness height.

Ozone deposition velocities in the model over land range from 0.4 to 0.8 cm s^{-1} during daytime, depending mainly on land type, and usually drop to zero at night; values over the oceans are typically 0.05 cm s^{-1} with no diel variation. The nighttime suppression of deposition over land is consistent with deposition flux observations at Harvard Forest, Massachusetts [J.W. Munger, unpublished data, 1993], which indicate that less than 10% of total O_3 deposition in summer takes place at night. Deposition velocities of NO_x and PANs are typically 30-50% lower than for O_3.

Subgrid Plumes

Chemical nonlinearities in urban and industrial plumes over North America are represented with the subgrid nested scheme of *Sillman et al.* [1990]. In that scheme, a 4°x5° grid box may contain two urban plume boxes in series (U1 and U2) and two power plant plume boxes in series (P1 and P2), representing aggregates of all major pollution plumes in the grid square (Figure 4). North American emissions are classified as "dispersed," "urban," or "power plant", based on emission data with 1/6°x1/4° resolution (≈ 20x20 km^2) representing the sum of the area and point source NAPAP inventories. A 1/6°x1/4° cell with NO_x emissions less than $1x10^{12}$ molecules cm^{-2} s^{-1} is dispersed; a cell with higher NO_x emissions is urban if its anthropogenic NO_x/NMHC emission ratio is less than 1 atom N per C atom and power plant otherwise. Emissions of NO_x from North America are classified in this manner as 54% dispersed, 21% urban, and 25% power plant. The classification is designed to optimize resolution of chemical nonlinearities [*Sillman et al.*, 1990], and may not describe the true nature of sources. Thus an industrial point source with low NO_x/NMHC emission ratio may be "urban," while a small point source may be "dispersed."

Urban and power plant emissions are injected in U1 and P1, where they react for 4 hours (one time step) in isolation from the rest of the grid box. At the beginning of the next time step the contents of U1 and P1 are transferred totally or in part to U2 and P2 where they dilute with rural air, receive dispersed emissions, and react in isolation for another 4 hours before being flushed to the rural box. Isoprene emissions in all plume boxes are equal to the grid box average.

The computation of plume box areas is described in Appendix C, and further details can be found in *Sillman et al.* [1990]. Boxes U1 and P1 include all 1/6°x1/4° urban and power plant cells within the 4°x5° grid square, and in addition the 0 to 4-hour fetches downwind of these cells. Boxes U2 and P2 represent the 4 to 8-hour old plumes. The plume boxes extend vertically from the surface to the local mixing depth and may thus cut across several (at most three) layers in the vertical.

Subgrid mass transfer in and out of plume boxes is implemented in equation (1) with the two operators S and S'. Operator S transfers all mass from plume boxes U2 and P2 to the rural box. Operator S' calculates new plume box volumes for U1, P1, U2, P2, transfers fractions f_U and f_P from the old boxes U1 and P1 to the new boxes U2 and P2, fills the rest of the new boxes U1, P1, U2,

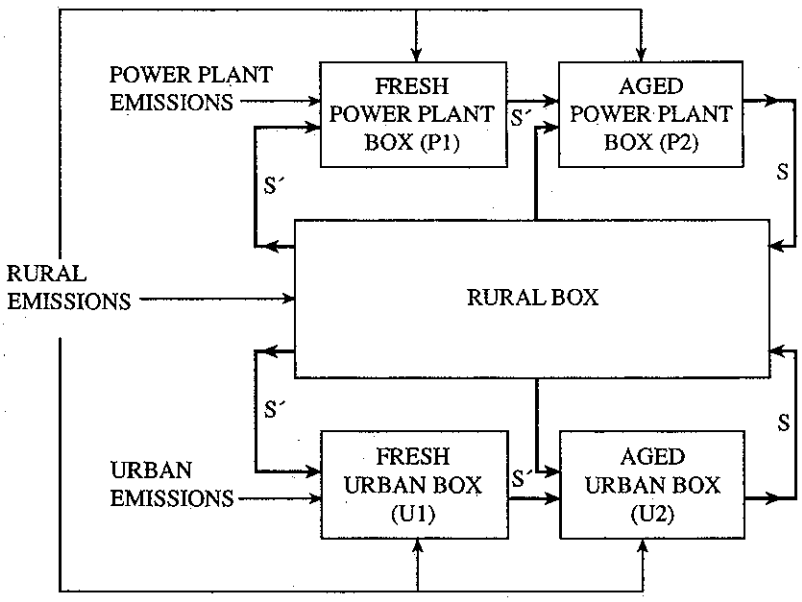

Fig. 4. Subgrid partitioning of a 4°x5° grid box into a rural box, two urban plume boxes in series (U1 and U2), and two power plant plume boxes in series (P1 and P2). Urban and power plant emissions are injected in boxes U1 and P1, respectively. Dispersed emissions are injected in all boxes in proportion to their rural areas. Thick lines indicate the mass fluxes enacted by the operators S and S'.

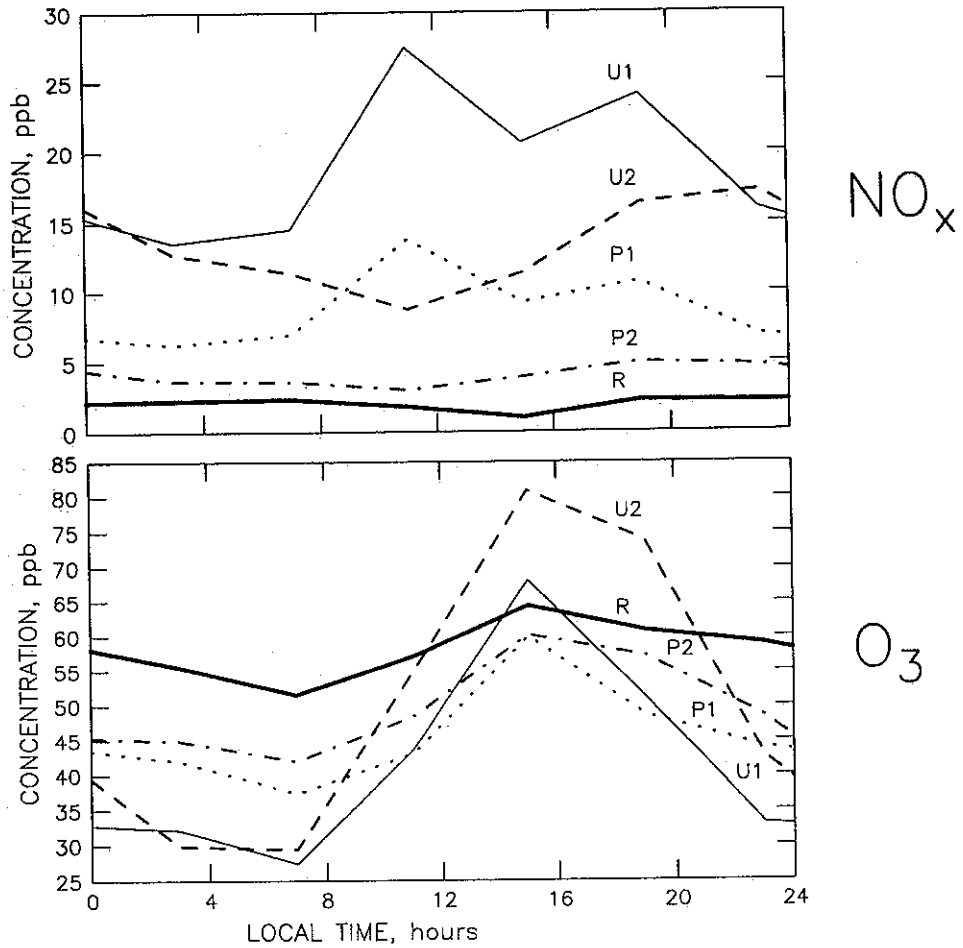

Fig. 5. Mean diel variations of NO_x and O_3 concentrations in the individual boxes of the New York grid box in August: rural (R), fresh urban plume (U1), aged urban plume (U2), fresh power plant plume (P1), and aged power plant plume (P2).

P2 with rural air, and adjusts for changes in mixing depth by detraining air from the plume boxes or entraining rural air. The fractions f_U and f_P are unity except under stagnant conditions (Appendix C). Transport of plume boxes across grid box boundaries is not allowed except for mixed layer convection; the operator T in equation (1) is applied only to rural air (rural box in Figure 4).

Figure 5 illustrates the functioning of subgrid plumes for the New York grid box. Subgrid plume boxes occupy on average 25% of total area in that grid square, a particularly large fraction (6% U1, 3% P1, 7% U2, 9% P2). Boxes U1 and U2 have respectively the highest concentrations of NO_x and O_3. Concentrations of NO_x in box P1 are lower than would be found in an actual power plant plume due to the forced dilution of emissions horizontally over the 20-km scale and vertically over the mixing depth. Nighttime concentrations of NO_x in the plume boxes are relatively low because of the 500-m mixing depth imposed by the model grid. Daytime concentrations of O_3 in the power plant plume boxes are low, despite high NO_x concentrations, because the high NO_x/NMHC ratio suppresses O_3 production. Nighttime concentrations of O_3 are low in all plume boxes because of titration by NO_x.

We find in the model that 29% of total NO_x emitted in the United States is oxidized within plume boxes, and that the plume boxes contribute 18% of the net O_3 produced in the U.S. boundary layer [*Jacob et al.*, this issue]. The net O_3 production efficiency, defined by *Lin et al.* [1988] as the net number of O_3 molecules produced (chemical production minus chemical loss) per molecule of NO_x oxidized, averages 3.3 for plume boxes and 7.5 for rural air in the U.S. boundary layer. The subgrid scheme thus captures substantial nonlinearity.

We conducted a sensitivity simulation without subgrid representation of plumes, i.e., with all emissions averaged over the 4°x5° grid. Net O_3 production in the U.S. boundary layer increased by 8%. Mean concentrations of O_3 in rural surface air increased by 5-12 ppb in the south central United States and by less elsewhere (Figure 6). This generally low sensitivity can be explained by the large contribution of dispersed sources to total NO_x emissions in the United States. The relatively large effect in the south central United States is due to a combination of high NO_x emissions from point sources (including industries along the Texas and Louisiana coasts) and high isoprene emissions. Entrainment of isoprene increases plume reactivity and magnifies small-scale nonlinearity [*Lin et al.*, 1988]. Without isoprene emission, we find that averaging emissions over the 4°x5° grid would cause only a 2-5 ppb increase in O_3 concentrations over the south central United States.

The effect of subgrid nonlinearity in our model is less than previously reported by *Sillman et al.* [1990] in boundary layer simulations for the northeastern United States with a subgrid representation of plumes similar to that used here. *Sillman et al.* [1990] found that averaging emissions over the 4°x5° grid resulted

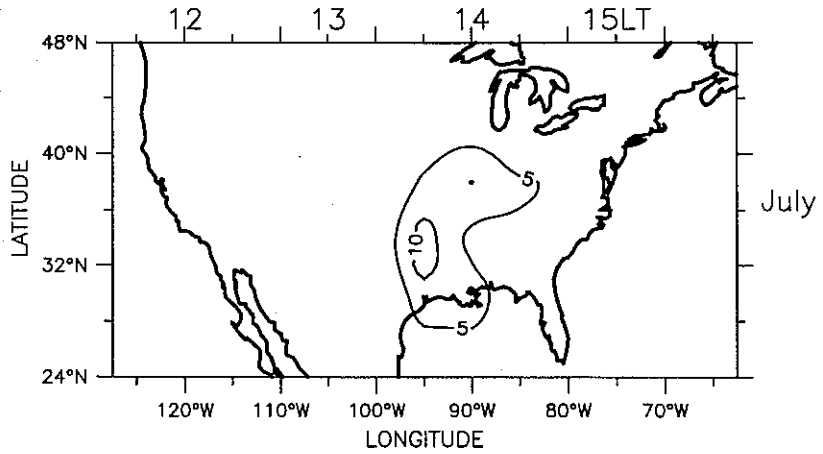

Fig. 6. Difference ($[O_3]_{4x5}$ - $[O_3]_{subgrid}$) of rural O_3 concentrations computed without subgrid plumes ($[O_3]_{4x5}$) versus with subgrid plumes ($[O_3]_{subgrid}$). Values are means for the lowest model layer (0-500 m above ground level) at 12-15 LT (Local Time) in July.

in a 8 ppb increase of afternoon O_3 concentrations. Their calculations were done for sunny, stagnant conditions, with an isoprene flux about 3 times higher than the mean used here for the same region. Pollution plumes under these conditions would be highly reactive and experience little dilution, resulting in particularly strong subgrid effects.

Results: Mean O_3 Distribution

Figure 7 (top panel) shows the mean afternoon concentrations of O_3 in rural air simulated for the lowest model layer (0-500 m) in July. Concentrations are highest over the south central United States, the eastern United States, and southern California, reflecting the distribution of NO_x emissions. Production of O_3 is primarily NO_x limited [*Jacob et al.*, this issue], although the relationship between O_3 production and NO_x emissions is nonlinear. Emissions of NO_x are highest in the northeastern U.S., but O_3 concentrations tend to be higher in the southeast because of stronger isoprene emission and greater insolation. The particularly high O_3 concentrations over the south central United States reflect high emissions of both NO_x and isoprene, combined with weak ventilation.

The bottom panel of Figure 7 shows the background O_3 concentrations originating from outside the continent. We derived this background in a simulation including no chemistry, i.e., with O_3 regulated solely by advection of boundary conditions and deposition. It ranges from less than 30 ppb over the Great Plains to 40 ppb along the east coast, reflecting differences in continentality and subsidence, and accounts for about half of mean O_3 concentrations in surface air over the eastern United States.

3. MODEL EVALUATION

Protocol

The GISS GCM is intended to simulate a typical meteorological year rather than any specific year; evaluation of model results with observations must therefore focus on seasonal statistics rather than on results for any particular day. The observations must be at rural sites distant from concentrated pollution sources since the subgrid plumes in the model are generic. The sites used for model evaluation are listed in Tables 4*a*-4*e* and their locations are shown in Figure 8. For O_3 we base our analysis on 18 U.S. sites selected by *Logan* [1989] for their rural character (Research Triangle Park, North Carolina, best described as suburban, is retained here as a member of the SURE network). The data records in Tables 4*a*-4*e* cover the period 1977-1991, during which secular trends of O_3 concentrations were negligible [*Lefohn et al.*, 1990; *National Research Council*, 1991]. Emissions of NO_x and NMHCs between 1977 and 1991 remained within 10% of 1985 values [*EPA*, 1991]. We use O_3 concentrations from June to August as a single statistical population for purposes of model evaluation, since there is no consistent seasonal trend over that period [*Logan*, 1985, 1989; *Vukovich and Fishman*, 1986; *Samson and Shi*, 1988; *Aneja et al.*, 1991; *Poulida et al.*, 1991]. The observations for O_3 precursors generally cover only a fraction of one summer, and we

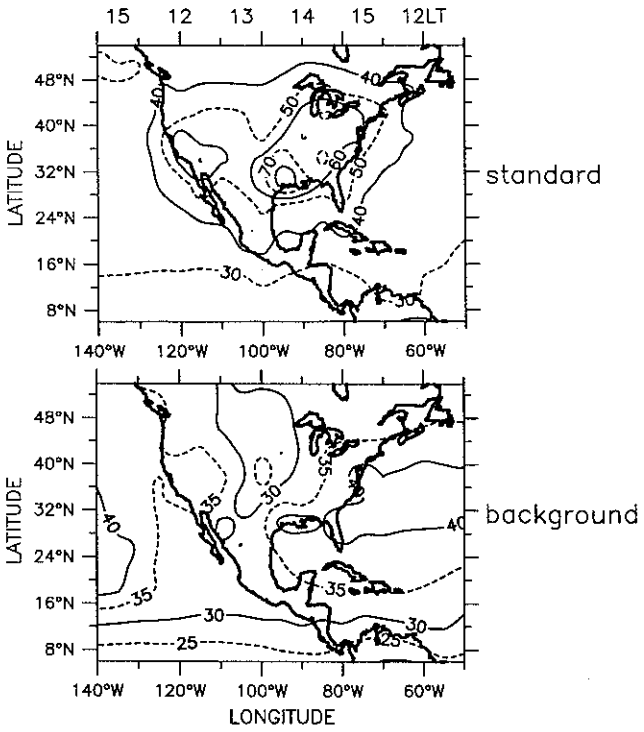

Fig. 7. Mean concentrations of O_3 (ppb) simulated in rural air for the lowest model layer (0-500 m above ground level) at 12-15 LT in July. The bottom panel shows the background O_3 originating from outside the continent, as computed by advection of boundary conditions in a simulation including deposition but no chemistry.

TABLE 4a. Rural O_3 Concentration Data Used for Model Evaluation

Site	Length of Record	Median (ppb)	Reference
1. Montague, MA (43°N, 73°W)	1978-1979	58	*Mueller and Hidy* [1983]
2. Scranton, PA (42°N, 76°W)	1978-1979	62	*Mueller and Hidy* [1983]
3. Indian River, DE (39°N, 76°W)	1978-1979	63	*Mueller and Hidy* [1983]
4. Duncan Falls, OH (40°N, 82°W)	1978-1979	63	*Mueller and Hidy* [1983]
5. Rockport, IN (38°N, 87°W)	1978-1979	63	*Mueller and Hidy* [1983]
6. Giles County, TN (35°N, 87°W)	1978-1979	58	*Mueller and Hidy* [1983]
7. Fort Wayne, IN (41°N, 85°W)	1978-1979	65	*Mueller and Hidy* [1983]
8. Research Triangle Park, NC (36°N, 79°W)	1978-1979	72	*Mueller and Hidy* [1983]
9. Lewisburg, WV (38°N, 80°W)	1978-1979	59	*Mueller and Hidy* [1983]
A. Whiteface Mountain, NY (44°N, 74°W)	1977-1983	42	*Lefohn and Mohnen* [1986]
B. Green Mountain National Forest, VT (45°N, 73°W)	1977,1980-82	40	*Evans* [1985]
C. Croatan National Forest, NC (35°N, 77°W)	1979-1982	45	*Evans* [1985]
D. Chequamegon National Forest, WI (45°N, 91°W)	1980-1982	40	*Evans* [1985]
E. Mark Twain National Forest, MO (37°N, 90°W)	1979,1981-1983	50	*Evans* [1985]
F. Kistachie National Forest, LA (32°N, 92°W)	1977,1982-1983	45	*Evans* [1985]
G. Custer National Forest, MT (45°N, 106°W)	1979-1982	50	*Evans* [1985]
H. Apache National Forest, AZ (34°N, 109°W)	1980-1983	45	*Evans* [1985]
I. Ochoco National Forest, OR (44°N, 120°W)	1980-1983	40	*Evans* [1985]
J. Harvard Forest, MA (43°N, 72°W)	1990-1991	47	J.W. Munger, unpublished, 1993

The medians are computed from the June to August records sampled at 1200 LT for site I; 1300 LT for sites G, H; 1400 LT for sites 5, 6, 7, D, E, F; 1500 LT for sites 1, 2, 3, 4, 8, 9, A, B, C, J. These sampling times correspond to the model time step ending at 2000 GMT. Sites 1-9 represent the Sulfate Regional Experiment (SURE) network. Concentrations at sites B-I are available with 5 ppb resolution only.

TABLE 4b. Rural CO Concentration Data Used for Model Evaluation

Site	Length of record	Median (ppb)	Reference
J. Harvard Forest, MA (43°N, 72°W)	June to Aug. 1990-1991	162	J.W. Munger, unpublished, 1993
K. Scotia, PA (40°N, 78°W)	July 16 to Aug. 31, 1988	215	*Parrish et al.* [1991]
L. Shenandoah National Park, VA (39°N, 79°W)	June to Aug. 1988	205	*Poulida et al.]* [1991]
M. Pride, LA (31°N, 91°W)	August 2-27, 1989	177	M.O. Rodgers, unpublished, 1993
N. Niwot Ridge, CO (40°N, 105°W)	July 24 to August 13, 1988	128	*Parrish et al.* [1991]

Medians are for 0800-1700 LT.

TABLE 4c. Rural NO_x Concentration Data Used for Model Evaluation

Site	Length of Record	Median (ppb)	Reference
J. Harvard Forest, MA (43°N, 72°W)	June to Aug. 1990-1991	0.66	J. W. Munger, unpublished, 1993
K. Scotia, PA (40°N, 78°W)	July 25 to Aug. 31, 1988	1.1	*Parrish et al.* [1993]
N. Niwot Ridge, CO (40°N, 105°W)	June to Aug. 1981,1983,1984	0.28	*Parrish et al.* [1990]
O. Bondville, IL (40°N, 88°W)	Aug. 16-30, 1988	1.2	*Parrish et al.* [1993]

Medians are for 0900 LT at site N, 1400 LT at site O, and 1500 LT at sites J and K. These sampling times correspond to the model time step ending at 2000 GMT, except at Niwot Ridge where a 0900 LT (1600 GMT) sampling time is chosen to minimize the influence of the Denver plume [*Parrish et al.*, 1990].

TABLE 4d. Rural PAN Concentration Data Used for Model Evaluation

Site	Length of Record	Median (ppb)	Reference
K. Scotia, PA (40°N, 78°W)	July 25 to Aug. 31, 1988	0.93	*Parrish et al.* [1993]
M. Pride, PA (31°N, 91°W)	Aug. 2-27, 1989	0.40	M.O. Rodgers, unpublished, 1993
O. Bondville, IL (40°N, 88°W)	Aug. 16-30, 1988	1.2	*Parrish et al.* [1993]
P. Elberton, GA (34°N, 83°W)	July 19 to Aug 20, 1991	0.70	M.O. Rodgers, unpublished, 1993

Medians are for 1400 LT at sites M, O, P, and 1500 LT at site K, corresponding to the model time step ending at 2000 GMT.

TABLE 4e. Rural HC2 Concentration Data Used for Model Evaluation

Site	Length of Record	Mean (ppbC)	Reference
K. Scotia, PA (40°N, 78°W)	18 Jul- 31 Aug 1988	13	H. Westberg, unpublished, 1993
Q. West Jefferson, MO (38°N, 93°W)	Jul-Aug 1980	49	*Vaughan et al.* [1982]
R. Robinson, IL (39°N, 88°W)	Jun-Jul 1977	33	*Sexton and Westberg* [1984]
S. Janesville, WI (43°N, 89°W)	Jul-Aug 1978	10	*Sexton and Westberg* [1984]
T. Belfast, ME (44°N, 69°W)	Jun-Jul 1975	7.5	*Sexton and Westberg* [1984]
U. Houston, TX (30°N, 95°W)	Aug 1978	6	*Sexton and Westberg* [1984]
V. Miami, FL (26°N, 80°W)	Jun-Jul 1976	4.5	*Sexton and Westberg* [1984]
W. Atlanta, GA (34°N, 84°W)	1985-1986	12	*McGregor and Westberg* [1990]
X. Dallas, TX (33°N, 97°W)	1985-1986	12	*McGregor and Westberg* [1990]
Y. Tulsa, OK (36°N, 96°W)	1985-1986	24	*McGregor and Westberg* [1990]

The measurements include C_{3-6} alkanes, ethylene, benzene, and toluene, except at site K (ethylene missing) and at sites T and V (aromatics missing). The mean at Scotia is computed from 204 grab samples collected between 0800 and 1700 LT over a 6-week period. The means at other sites are computed from 8-25 samples collected at the surface or from low-flying aircraft during daytime hours. Measurements at sites U-Y were collected outside the urban plume.

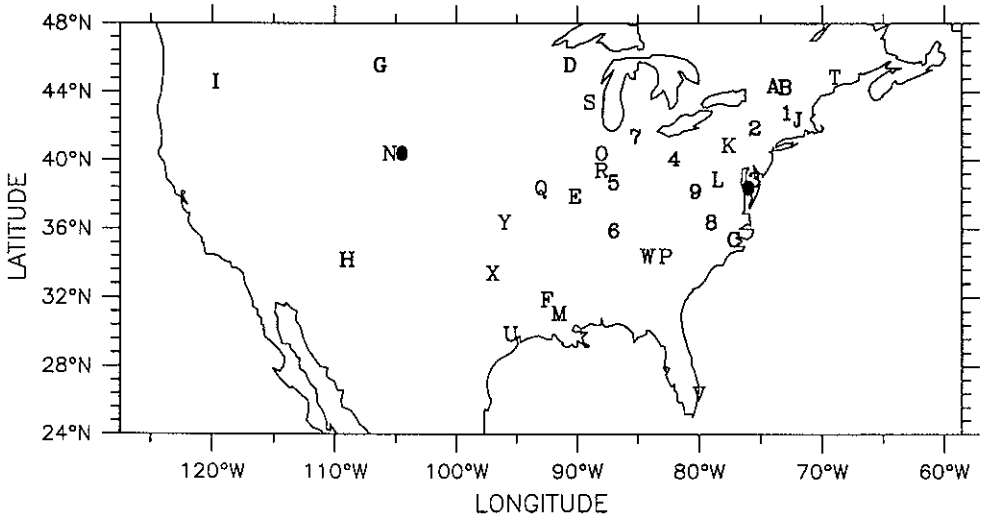

Fig. 8. Sites used for model evaluation (see Tables 4*a*-4*e* for identification and reference). Boulder and Wallops Island are indicated by black circles.

compare them to monthly statistics for the corresponding model months.

Surface measurements are useful for model evaluation only in daytime, when the surface air is representative of a fairly deep mixed layer that can be resolved by the model [*Jacob and Prather*, 1990; *McKeen et al.*, 1991; *Hastie et al.*, 1993; *Parrish et al.*, 1993]. For O_3, NO_x, and PAN we restrict our attention to 12-15 LT (Local Time), when the mixed layer is usually at its maximum depth. The model gives one value per day in that time window, the exact hour depending on longitude (12 LT on the west coast of the United States, 15 LT on the east coast), and we sample the time series of observed hourly mean concentrations at that particular local time. For CO and HC2 we use data for 8-17 LT to match the format of published observations.

Seasonal medians are preferable to means for evaluating model results with surface observations, as observed means may be skewed by local pollution [*Parrish et al.*, 1993]. We extract the medians and other quantiles of the probability distribution for rural sites in the model by merging the time series of concentrations in rural air and in the aged plume boxes on an area-weighted basis, assuming random influence of pollution plumes over rural areas (Appendix D). The plume boxes have negligible effect on model medians but modify slightly the higher quantiles.

Surface Ozone: Medians

Figure 9 compares simulated and observed summer median afternoon O_3 concentrations at 19 rural sites in the United States (the 18 sites of *Logan* [1989] and Harvard Forest). The correlation coefficient between model and observations is $r = 0.72$, reflecting largely the contrast between high concentrations in the densely populated region of the eastern United States (sites 1-9) and relatively low concentrations outside that region. The model overpredicts the observed medians by 4 ppb on average; such a small difference could reflect the deposition-driven gradient between the lower mixed layer (sampled by the model) and the surface layer (sampled by the observations) [*Van Valin et al.*, 1991]. There is a major regional discrepancy in the south central United States (sites 6, E, F), where simulated concentrations are 13-19 ppb too high. We confirmed the discrepancy with additional observations from nonurban sites in eastern Texas, Oklahoma, and Arkansas, available through the aeronometric information retrieval system (AIRS) of the EPA; model results at these sites are typically 15-20 ppb too high. A detailed analysis of the AIRS data by *Vukovich and Fishman* [1986] indicates that the south central United States can in some years experience monthly mean daily maximum O_3 concentrations in excess of 70 ppb; model results in that region may thus fall within the range of interannual variability, but they are atypical.

One likely explanation for the overprediction in the south central United States is that inflow of tropical maritime air from the Gulf of Mexico is suppressed in the GCM by an anomalously weak pressure gradient along the Gulf coast [*Jacob and Prather*, 1990]. The same meteorological anomaly is apparent in the mean pressure maps for July 1978, when observed O_3 concentrations over the south central U.S. were unusually high [*Vukovich and Fishman*, 1986]. Suppression of the maritime inflow reduces ventilation and results in high temperatures and high insolation, stimulating O_3 production and compounding the effect of the weak ventilation.

The overprediction of O_3 concentrations over the south central United States could also reflect insufficient resolution of NO_x point sources. Model results in that region are particularly sensitive to subgrid nonlinear chemistry, as discussed above; it may be that the minimum 20x20 km^2 averaging of point sources in our subgrid scheme is too coarse to capture the nonlinearity fully. It may also be that the averaging of isoprene emission over the 4°x5° grid exaggerates entrainment of isoprene in plumes from NO_x point sources along the Gulf coast. The regional photochemical model of *McKeen et al.* [1991], operating with a 60x60 km^2 resolution, also overpredicts O_3 concentrations in the south central United States. Excessive dilution of NO_x point sources may be a problem in both models.

Surface Ozone: Variance

Figure 10 compares the simulated and observed probability distributions of afternoon O_3 concentrations at three U.S. sites. There is more variance in the eastern U.S. than in the west, both in the model and in the observations, reflecting the episodic nature of pollution in the east [*Logan*, 1989]. The variance in the model is less than observed, as may be expected due to spatial averaging over the model grid. The low tail in the observations at Harvard

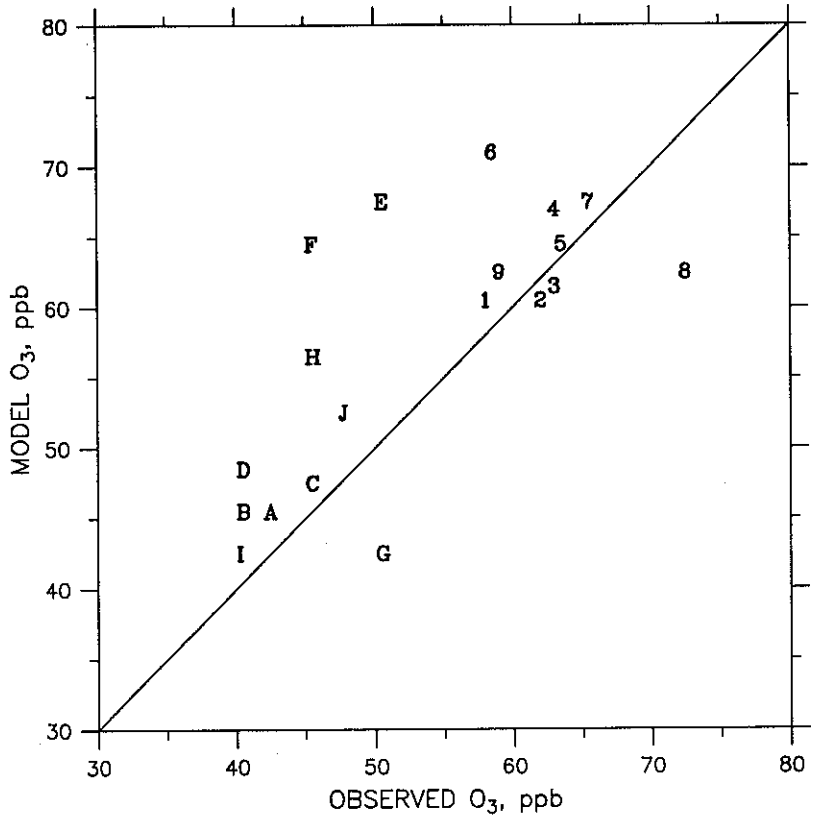

Fig. 9. Simulated versus observed median afternoon concentrations of O_3 at 19 rural U.S. sites in June to August (Table 4*a*). The medians are computed from the time series of concentrations sampled at 12-15 LT depending on the longitude of the site (see footnote to Table 4*a*).

Forest ([O_3] < 40 ppb) is associated with either rain or polar air. Rain suppresses mixing of the surface layer, an effect that is not resolved by the model, and intrusions of clean polar air are not well resolved either because the boundary conditions at 56°N represent mean observations from subpolar ozonesonde stations.

A more relevant test of the model variance is the ability to simulate regional high-O_3 episodes over the eastern United States. *Logan* [1989] presented seasonal episode statistics derived from O_3 concentration data at the nine SURE sites and Whiteface Mountain (sites 1-9 and A). She defined an episode as the occurrence of mean 10-16 LT O_3 concentrations in excess of 70 ppb at four or more of these 10 sites for two or more consecutive days. She found five episodes in June to August of each of 1978 and 1979, with each episode lasting from 2 to 5 days, for a total of 15 episode days each summer. The same analysis in the model summer indicate four episodes, each lasting from 3 to 9 days, for a total of 21 episode days. The frequency of regional O_3 episodes in the model is consistent with observations, although the model episodes tend to be longer than observed.

It is well known that regional O_3 episodes over the eastern United States are associated with weak, stagnant, warm anticyclones [*Decker et al.*, 1976; *Altshuller*, 1978; *Wolff and Lioy*, 1980]. This association is well reproduced by the model, as illustrated in Figure 11 with a case study for August 16-21 of the GCM summer. On August 16, O_3 concentrations are low over most of the eastern U.S. because of a high-pressure ridge extending from northern Canada to Kentucky. During the next few days the high-pressure migrates eastward and progressively decays, causing regional stagnation. Ozone accumulates on the back side of the high pressure as the slow anticyclonic flow passes over major source regions. Peak concentrations occur over Michigan on August 19, and over New York on August 21. By August 21, Michigan is already ventilated by a strong anticyclone that traveled from western Canada to Minnesota over the previous two days.

Anticyclones in the GCM travel along a preferred track from central Canada to the mid-Atlantic seaboard across the northeastern U.S., consistent with observations [*Harman*, 1987]. Not all anticyclones passing over the northeastern U.S. generate regional O_3 episodes, either in the model or in the observations. Important variables determining the occurrence of a regional O_3 episode are the persistence, pressure, and temperature of the anticyclone [*Logan*, 1989]; pressure is important because weak anticyclones are associated with regional stagnation. We derived quantitative criteria for predicting regional O_3 episodes in the observations by using 1978-1979 data for anticyclone tracks over the eastern U.S. [*National Oceanic and Atmospheric Administration (NOAA)*, 1978, 1979] and concurrent statistics of O_3 episodes from *Logan* [1989]. Results in Figure 12 show that regional O_3 episodes are most likely to occur when anticyclones stagnate over the eastern U.S. or immediately offshore for $N > 3$ days, with anticyclone MSL pressure $P < 1025$ mbar and afternoon surface air temperature $T > 298$ K. The same criteria diagnose successfully the development of regional O_3 episodes in the model (Figure 12), implying that the model generates episodes for the right reasons. Both the observations and the GCM show significant negative correlation between P and T ($r = -0.44$ in the observations) and no correlation of anticyclone persistence (N)

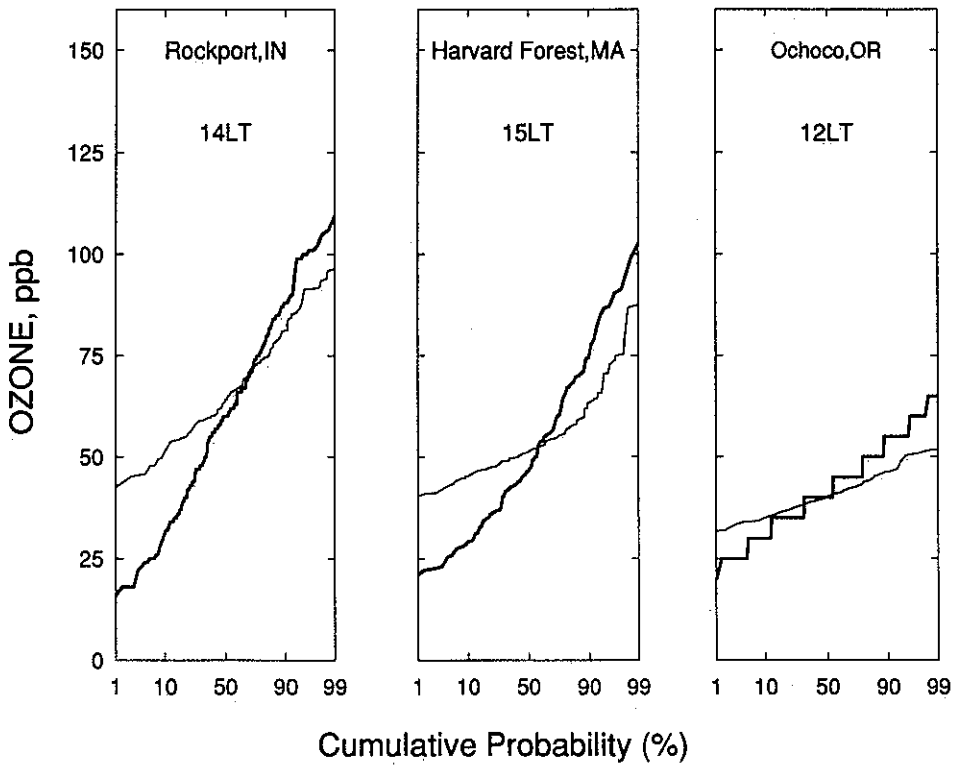

Fig. 10. Cumulative probability distributions of afternoon O_3 concentrations at three rural U.S. sites in June to August (Table 4*a*). Model results (thin lines) are compared to observations (thick lines). The abscissa is such that a normal distribution would plot as a straight line (probability scale).

with either P or T. We argue in the companion paper that stagnation rather than temperature is the primary driving force for the development of regional O_3 episodes.

Ozone at Altitude

Long-term ozonesonde records are available at Boulder, Colorado from NOAA [*Oltmans et al.*, 1989; *S. J. Oltmans*, personal communication, 1993] and at Wallops Island, Virginia from the National Aeronautics and Space Administration (NASA). Figure 13 compares the simulated and observed summer mean O_3 concentrations at these two sites. The short dashes show the model background, as defined by advection of boundary conditions in a simulation including deposition but no chemistry. Significant U.S. pollution enhancement in the model extends up to 500 mbar over Boulder and up to 700 mbar over Wallops Island. Boundary layer concentrations over Boulder are underpredicted by 5-10 ppb, perhaps because of the suburban nature of the site. Concentrations over Wallops Island are underpredicted by about 10 ppb throughout the tropospheric column, but this discrepancy could reflect in part the calibration of the measurements. A laboratory calibration by *Barnes et al.* [1985] indicates that the NASA sondes are 8-14% too high at 800-300 mbar, and a field calibration by *Hilsenrath et al.* [1986] indicates 2% and 12% positive biases for the NOAA and NASA sondes, respectively. The NOAA ozonesonde data are shown here on a scale 2.5% lower than the data obtained in the *Hilsenrath et al.* [1986] calibration.

Carbon Monoxide

Figure 14 compares simulated and observed median daytime concentrations of CO at five rural U.S. sites (Table 4*b*). The agreement is good (correlation coefficient r = 0.93). Concentrations at Niwot Ridge, Colorado, 3100-m altitude (site N) reflect mainly the advection of boundary conditions from the Pacific; concentrations at eastern U.S. sites are higher because of regional sources. The sources of CO in the U.S. boundary layer in the model include direct emission (47% of total source), isoprene oxidation with 60% yield (27%), CH_4 oxidation with 90% yield (17%), and oxidation of anthropogenic NMHCs with 30-60% yield (10%). Isoprene oxidation is particularly important in the southeast, as may be inferred from Figure 3.

It has been argued that the NAPAP inventory underestimates CO emissions from mobile sources [*Lawson et al.*, 1990; *Pierson et al.*, 1990]. We conducted a sensitivity simulation with CO emissions increased uniformly by 50%, corresponding roughly to a doubling of emissions from mobile sources. Results shown as arrows in Figure 14 indicate improved simulation in the southeast (sites L and M) but degraded simulation in the northeast (sites J and K).

Nitrogen Oxides

Figure 15 compares simulated and observed median afternoon concentrations of NO_x and PANs at rural U.S. sites (Tables 4*c-d*). Concentrations of NO_x are underpredicted by 10% to 30%, a small discrepancy that could reflect a number of factors including operator splitting in the model. Concentrations of PANs are overpredicted by a factor of 2 to 3, a more serious discrepancy. The measurements are for peroxyacetylnitrate (PAN), while model results are for total peroxyacylnitrates (PANs). However, mass balances for total reactive nitrogen oxides (NO_y) in the observations indicate that the concentrations of higher peroxyacylnitrates are low relative to PAN [*Buhr et al.*, 1990; *Parrish et al.*, 1993].

The overprediction of PANs appears to reflect at least two

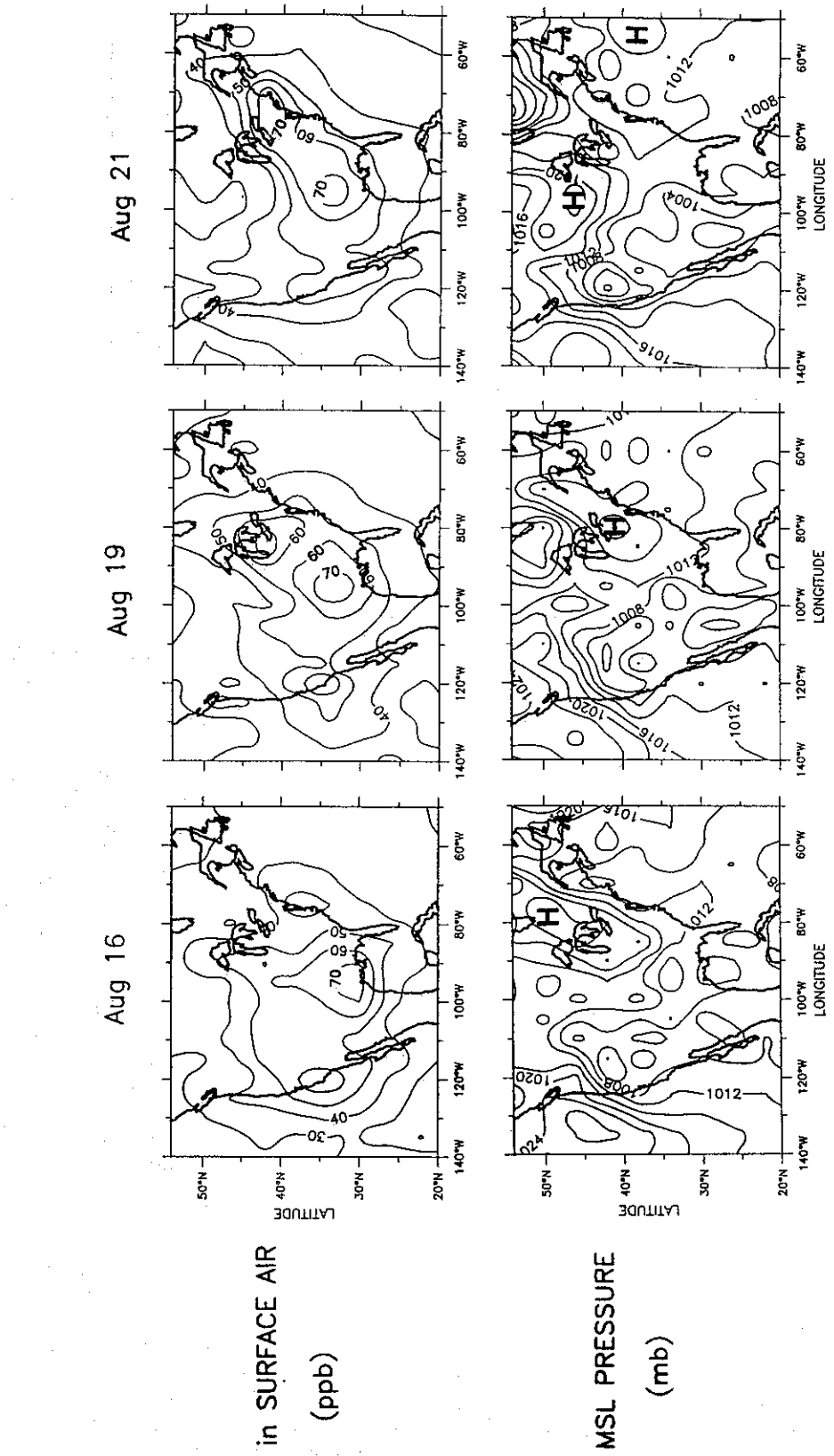

Fig. 11. Development of a regional O_3 episode over the northeastern U.S. in the model. The Fig. shows the 24-hour average rural O_3 concentrations (ppb) in the lowest model layer (0-500 m above ground level) on August 16, 19, and 21 of the GCM year, and the corresponding mean sea level pressures (mbar) in the GCM.

problems in the *Lurmann et al.* [1986] mechanism. First is excessive production of higher peroxyacylnitrates; calculations using the mechanism indicate typically a 30-40% contribution of higher peroxyacylnitrates to rural PANs [*Sillman*, 1988], but the observations suggest a lower contribution. It is assumed in the mechanism that all peroxyacylnitrates have the same formation and destruction rates as PAN, however the lifetimes of the higher peroxyacylnitrates could be short due to rapid thermal decomposition or oxidation by OH [*Trainer et al.*, 1991]. A second problem in the *Lurmann et al.* [1986] mechanism is excessive production of PAN from oxidation of isoprene. Under high-NO_x conditions, as in the boundary layer over the eastern U.S., the mechanism yields 0.59 peroxyacetyl radicals (precursor of PAN) from the oxidation of one molecule of isoprene, whereas laboratory measurements [*Tuazon and Atkinson*, 1989, 1990*ab*] indicate a yield of only 0.31.

Part of the overprediction of PANs could also be due to an underestimate of deposition. *Shepson et al.* [1992] recently reported the rapid nighttime depletion of PAN at a rural site in Canada under relatively cold conditions, and concluded that the PAN deposition velocities presently used in models are too low. We conducted a sensitivity simulation assuming zero surface resistance of PANs to deposition. The simulated concentrations of PANs fell to values consistent with observations, while the NO_x concentrations for the sites in Figure 15 decreased by less than 0.1 ppb. Surface concentrations of O_3 decreased by 2-7 ppb over the United States, with strongest effects in the south central region, reflecting in part the radical loss from PANs deposition. It thus appears that enhanced deposition of PANs would improve not only the simulation of PANs but also that of O_3 over the south central United States, while having relatively little effect on other model results.

Hydrocarbons

Figure 16 compares simulated and observed daytime concentrations of the anthropogenic tracer HC2 at 10 rural U.S. sites (Table 4*e*). The most extensive record is at Scotia (site K). Model results are consistent with observations, except for the three central United States sites (Q, R, Y) where concentrations are underpredicted by factors of 2 to 6. The origin of the discrepancy is unclear. Measured hydrocarbon ratios at these sites show no obvious influence of fresh pollution. *Pierson et al.* [1990] argue that the NAPAP inventory underestimates NMHC emissions from mobile sources by a factor of about 4; increasing NMHC emissions in the model would improve the simulation at the three central U.S. sites but degrade the simulation elsewhere (and in particular at Scotia).

Model results for HC1 (mainly isoprene) are not comparable to surface measurements because of the steep gradient between the surface layer and the mixed layer [*Trainer et al.*, 1987]. We focus

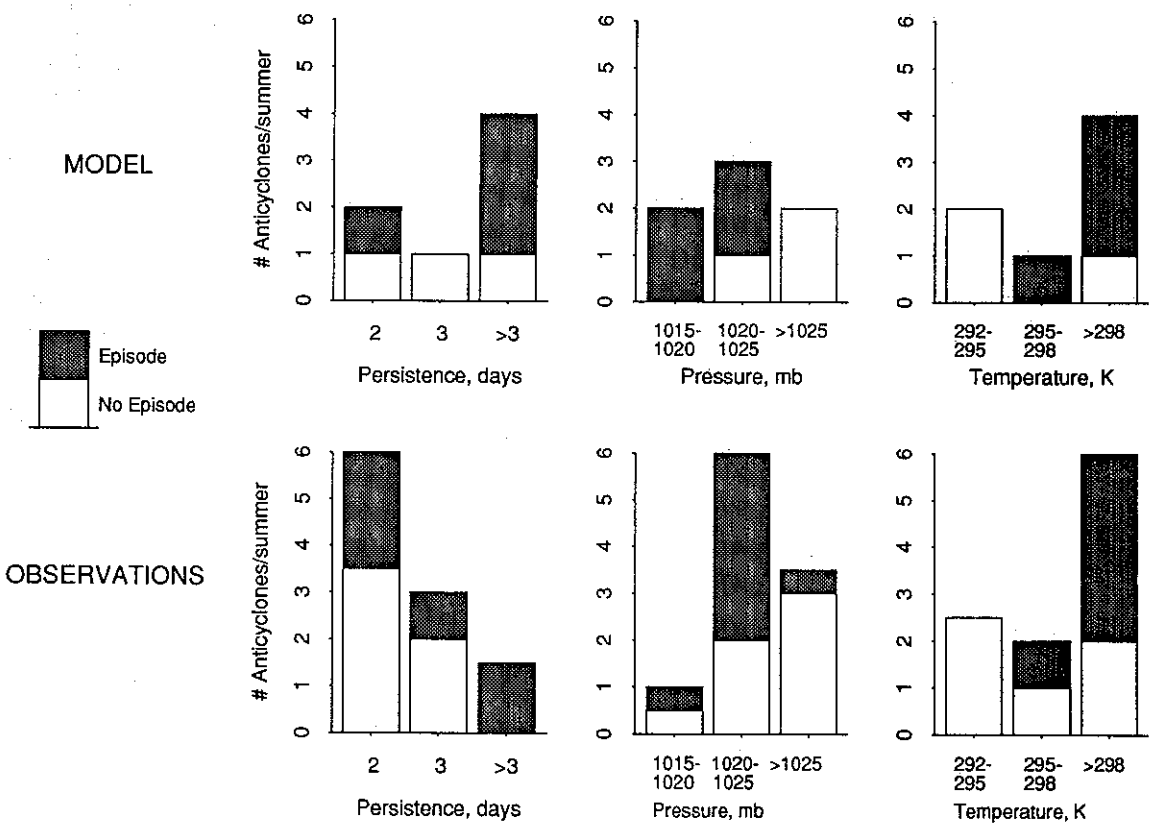

Fig. 12. Criteria for the occurrence of regional O_3 episodes in association with anticyclone passages over the eastern U.S. in June to August. All anticyclones persisting for $N \geq 2$ days over the eastern United States or immediately offshore (between 32°N and 44°N and between 90°W and 65°W) are diagnosed for the occurrence of a regional O_3 episode based on the criteria of *Logan* [1989]. The diagnosis is then related to three anticyclone variables: (1) the number N of days of persistence of the anticyclone over the eastern U.S., (2) the mean anticyclone pressure P during the N days, and (3) the mean 14 LT surface temperature T during the N days at the four SURE sites experiencing the highest O_3 concentrations. Model results for the GCM summer are compared to two summers of observations (1978-1979). Anticyclone data for 1978-1979 are from *NOAA* [1978, 1979], and corresponding data for regional O_3 episodes are from *Logan* [1989].

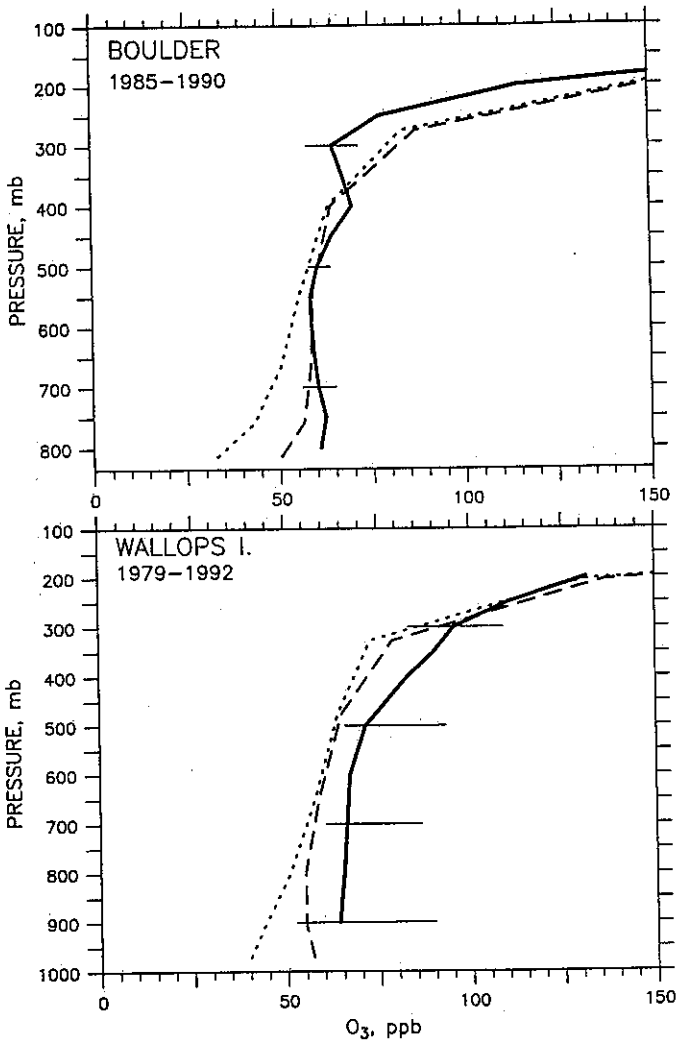

Fig. 13. Mean O_3 concentrations over Boulder, Colorado, and Wallops Island, Virginia, in June-August. Ozonesonde observations (solid lines) are compared to model results (long-dashed lines). The short-dashed lines show the model background representing advection of boundary conditions in a simulation with deposition but no chemistry. The ozonesonde observations include 50 soundings in 1985-1990 at Boulder and 126 soundings in 1979-1992 at Wallops Island. The horizontal bars show the interannual ranges of the observed means. The ozonesondes were launched at various times of day, mostly between 9 and 14 LT; model results are 24-hour averages. The mean surface pressure at Boulder is 835 mbar.

our attention on balloon measurements made over an Alabama forest by P.R. Zimmerman during the Regional Oxidants in the Southern Environment (ROSE) program in July 1990. The median 12-16 LT isoprene concentration measured at 100 to 350-m altitude was 9.9 ppbC (10 days of observations). We find in the model a median isoprene concentration of 2.8 ppbC at 14 LT for that grid box in July, i.e., a factor of 3.5 lower than observed. Model output for isoprene is affected by operator splitting, as discussed above; we made an independent estimate of the isoprene concentration in the model by using model values for the emission flux from deciduous forest canopies (3.6×10^{12} atoms C cm^{-2} s^{-1} at 303 K and full sun) and the local OH concentration (6×10^6 molecules cm^{-3} at noon), and assuming a 1-km scale height for isoprene [*Rasmussen and Khalil*, 1988]. The resulting steady state isoprene concentration in the lower mixed layer is 3.6 ppbC, still much lower than observed.

A likely reason for the underprediction of isoprene at the ROSE site is that local emission is underestimated. *Guenther et al.* [1993] report a light-saturated isoprene emission of 6.7×10^{12} molecules cm^{-2} s^{-1} at 303 K for the site, i.e., twice the value in the model, reflecting the high abundance of oak and sweetgum. Considering that O_3 production is primarily NO_x limited, a factor of 2 uncertainty in isoprene emission has little effect on model results. We conducted a sensitivity simulation with isoprene emissions doubled uniformly from the standard model and found less than a 4 ppb increase in mean O_3 concentrations anywhere.

An additional explanation for the underprediction of isoprene at the ROSE site may be that OH concentrations in the model are too high. The few direct measurements of OH concentrations in rural air suggest values about a factor of 2 lower than computed from photochemical models [*Perner et al.*, 1987; *Mount and Eisele*, 1992]. A decrease of OH concentrations in the model could make results for HC2 consistent with an underestimate of HC2 emissions in the NAPAP inventory. Concentrations of NO_x would be overpredicted, however. The effect on O_3 production would depend on the nature of the missing term in the OH budget [*Ridley et al.*, 1992].

4. Conclusions

A three-dimensional, continental scale photochemical model has been used to simulate the concentrations of O_3 and its precursors over North America for three summer months. The model reproduces well the median afternoon concentrations of O_3 observed at rural sites, to within 5 ppb in most cases, and captures successfully the development of regional high-O_3 episodes in the northeastern United States on the back side of weak, warm, stagnant anticyclones. A problem area is the south central United States, where simulated O_3 concentrations are 15-20 ppb higher than observed. This overprediction is explained in part by weaker-than-normal ventilation of the region in the GCM and may also reflect insufficient resolution of point sources along the Texas and Louisiana coasts. Subgrid representation of pollution plumes has little effect on mean O_3 concentrations in the model, except in the south central United States where point sources represent a large fraction of total NO_x emissions and where photochemical aging of plumes is particularly rapid due to high concentrations of isoprene.

Simulated concentrations of CO and NO_x are in good agreement with rural observations, but concentrations of PANs are overpredicted by a factor of 2 to 3. This overprediction is due at least in part to flaws in the chemical mechanism, including excessive stability of peroxyacylnitrates other than PAN and excessive production of PAN from oxidation of isoprene. It could also reflect in part an underestimate of PANs deposition. Improved understanding of the production and fate of PANs in continental boundary layers is needed in view of the implications for the source of NO_x in the remote troposphere [*Crutzen*, 1979; *Singh*, 1987].

Appendix A: Parameterization of the Chemical Computation

The polynomials used to compute *(P–L)* in the model are constructed by least squares fit to results from a large number of photochemical box model calculations sampling randomly the atmospheric ranges of the 11 independent variables in Table 3 [*Spivakovsky et al.*, 1990b]. The polynomials include 200-500

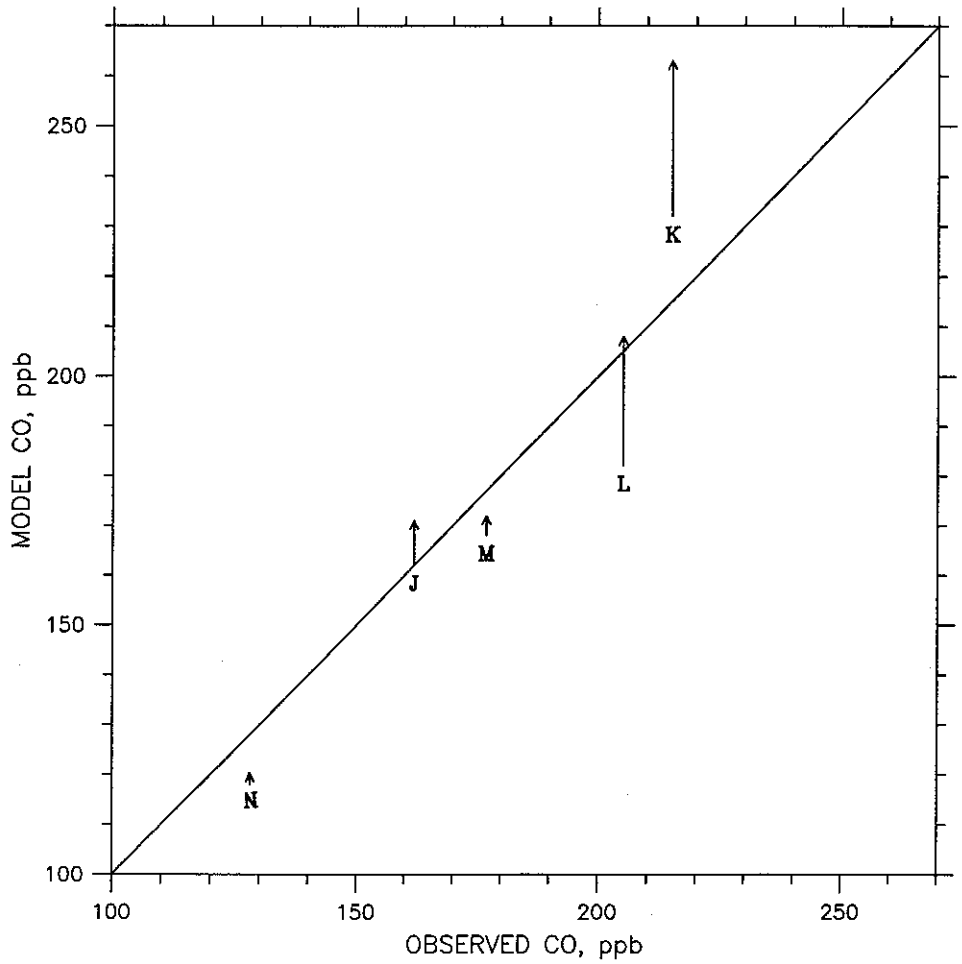

Fig. 14. Simulated versus observed median daytime (8-17 LT) concentrations of CO at five rural U.S. sites (Table 4*b*). The arrows point to the concentrations calculated in a sensitivity simulation with CO emissions increased by 50% from the NAPAP inventory values, corresponding roughly to a doubling of automobile emissions. Model results for Niwot Ridge (point N, 3100-m altitude) are sampled in layer 3, corresponding to the altitude of the site relative to the mean terrain elevation of the grid square.

selected terms up to the sixth order and cross terms up to the fourth-order. About 4000 photochemical box model calculations [*Jacob et al.*, 1989] are used to construct each polynomial. Separate sets of polynomials are constructed for day and night and for the lower troposphere (>800 mbar), the middle troposphere (800-500 mbar), and the upper troposphere (500-200 mb). The lower troposphere is subdivided further into four ranges of NO_x concentrations: 0.001-0.1 ppb, 0.1-2 ppb, 2-20 ppb, and 20-100 ppb. Additional sets of polynomials are constructed for subgrid plume boxes [*Jacob et al.*, 1989].

The quality of the parameterization fit is evaluated with the root-mean-square error (rms):

$$\text{rms} = \frac{\left(\frac{1}{n}\sum_{k=1}^{n}(y_k - Y_k)^2\right)^{1/2}}{\frac{1}{n}\sum_{1}^{n} Y_k} \qquad \text{(A1)}$$

where n is the number of photochemical box model calculations used to construct the parameterization, Y_k is the value of the output variable in calculation k, and y_k is the corresponding approximation computed from the polynomial. The rms of the chemical parameterizations are < 17% in the lower troposphere and < 25% in the middle and upper troposphere. The rms of the radiative parameterizations are less than 3%.

APPENDIX B: ISOPRENE EMISSION

The isoprene emission flux ψ from an isoprene-emitting leaf, per unit area of leaf surface, is computed as a function of local air temperature (T) and solar radiation flux (I):

$$\psi = \psi_o\, f(T) g(I) \qquad \text{(B1)}$$

where $\psi_o = 1.1\text{x}10^{12}$ atoms C cm^{-2} leaf s^{-1} is a universal flux at 298 K under light saturated conditions, based on a mean value of $1.1\text{x}10^{14}$ atoms C g^{-1} leaf s^{-1} from *Lamb et al.* [1987] and assuming a leaf density of 100 g m^{-2}. The functions $f(T)$ and $g(I)$ are from *Lamb et al.* [1987] and *Tingey et al.* [1979], respectively,

$$f(T) = e^{\alpha(T-298)} \qquad \text{(B2)}$$

$$g(I) = \exp\left[a\left(\frac{1}{1+e^{-b(I-c)}} - 1\right)\right] \qquad \text{(B3)}$$

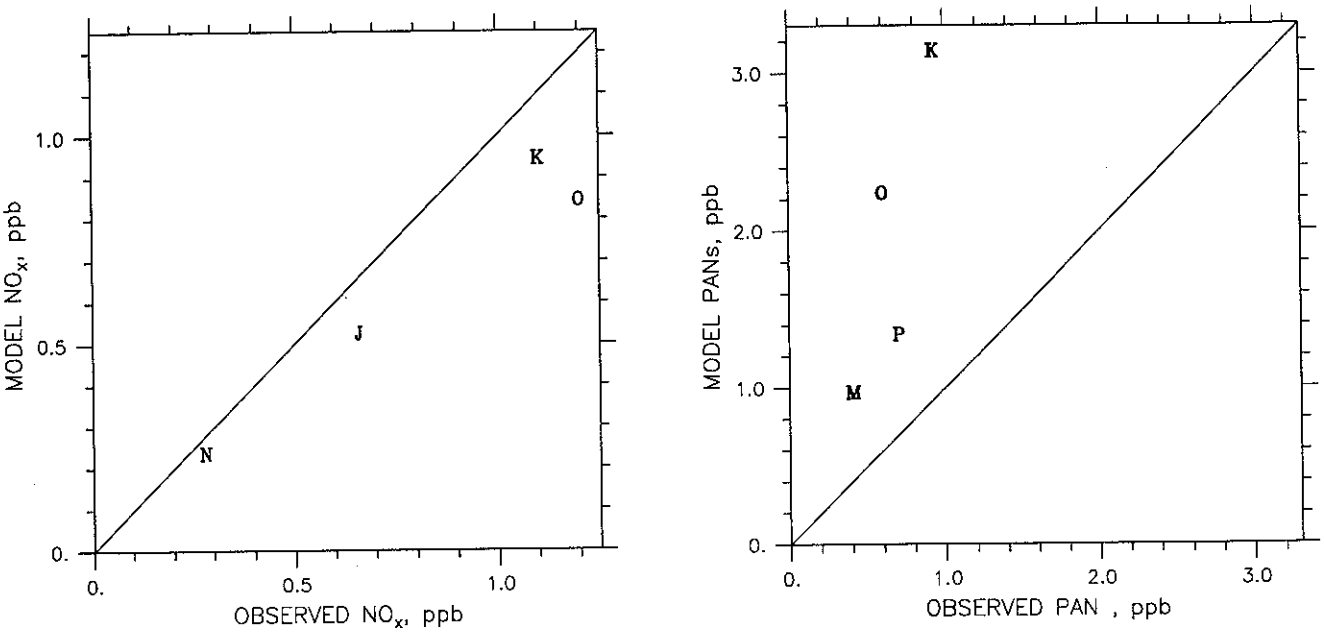

Fig. 15. Simulated versus observed median afternoon concentrations of NO_x and PANs at rural U.S. sites (Tables 4*c*-*d*). The medians are computed from the time series of concentrations sampled at 14 or 15 LT depending on the longitude of the site. An exception is Niwot Ridge (point N) where the time series are sampled at 9 LT to minimize the influence of the Denver urban plume in the observations [*Parrish et al.*, 1990].

with coefficients $\alpha = 0.096\ K^{-1}$, $a = 10.2$, $b = 0.029\ m^2\ W^{-1}$, and $c = 2.4\ W\ m^{-2}$. The temperature in the canopy is derived from the 5-day mean GCM temperature at ≈ 250 m above ground (middle of lowest layer) by assuming an adiabatic lapse rate and prescribing a typical diel cycle (Table 1).

Integration of (B1) over the canopy depth yields the total isoprene emission ϕ per unit area of the Earth's surface:

$$\phi = F\,\psi_o\,L\,\omega\,e^{\alpha(T-298)} \qquad \text{(B4)}$$

Here F is the areal fraction of leaf biomass that emits isoprene (assumed independent of altitude), L is the total leaf area index of the canopy, and ω is a light correction factor:

$$\omega = \frac{1}{L}\int_0^L g(I)\,dL' \qquad \text{(B5)}$$

where I is attenuated by the leaf area index overhead L'. We view the canopy as a grey absorber with light extinction coefficient $k = 0.5$ normalized to the leaf area index [*Verstraete*, 1987]:

$$I = I^o e^{-kL'/\cos\theta} \qquad \text{(B6)}$$

where I^o is the solar radiation flux at canopy top (specified by the GCM) and θ is the solar zenith angle. Figure B1 shows the resulting values of ω as a function of I^o and $kL/\cos\theta$.

Values of F and L are taken from *Lamb et al.* [1987] and *Lieth* [1975], respectively, for the different vegetation types of the *Matthews* [1983] 1°x1° map. The highest isoprene emissions are for tropical and deciduous forests. The emission computed for a deciduous forest canopy under light-saturated conditions at 303 K is 3.6×10^{12} atoms C $cm^{-2}\ s^{-1}$, in excellent agreement with canopy measurements for a mixed hardwood forest at Harvard Forest, Massachusetts [*Goldstein et al.*, 1992]. *Guenther et al.* [1993] give mean light-saturated emission fluxes at 303 K of 6.2×10^{12} atoms C $cm^{-2}\ s^{-1}$ for deciduous forests in the United States and 4.1×10^{12} atoms C $cm^{-2}\ s^{-1}$ for all U.S. woodlands, higher than assumed here. The uncertainty on isoprene emission has little effect on computed O_3 concentrations, as discussed in the text.

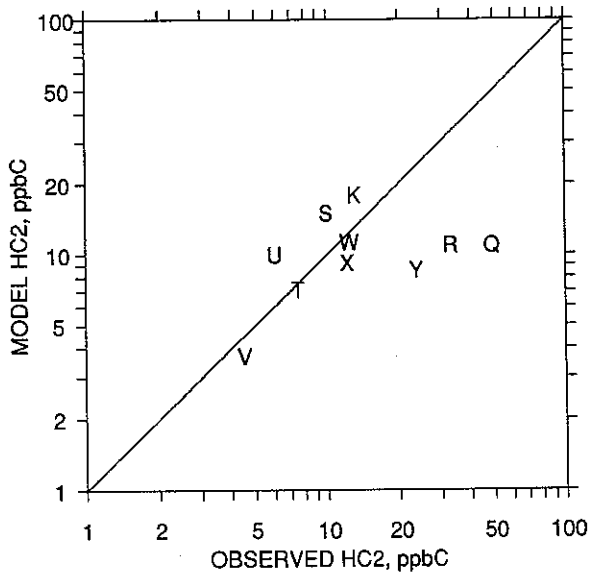

Fig. 16. Simulated versus observed mean daytime concentrations of HC2 at 10 rural U.S. sites (Table 4*e*). The observations at Scotia (point K) are means for 8-17 LT; the observations at other sites are means of samples collected at various daytime hours. Model results at all sites are means for 8-17 LT.

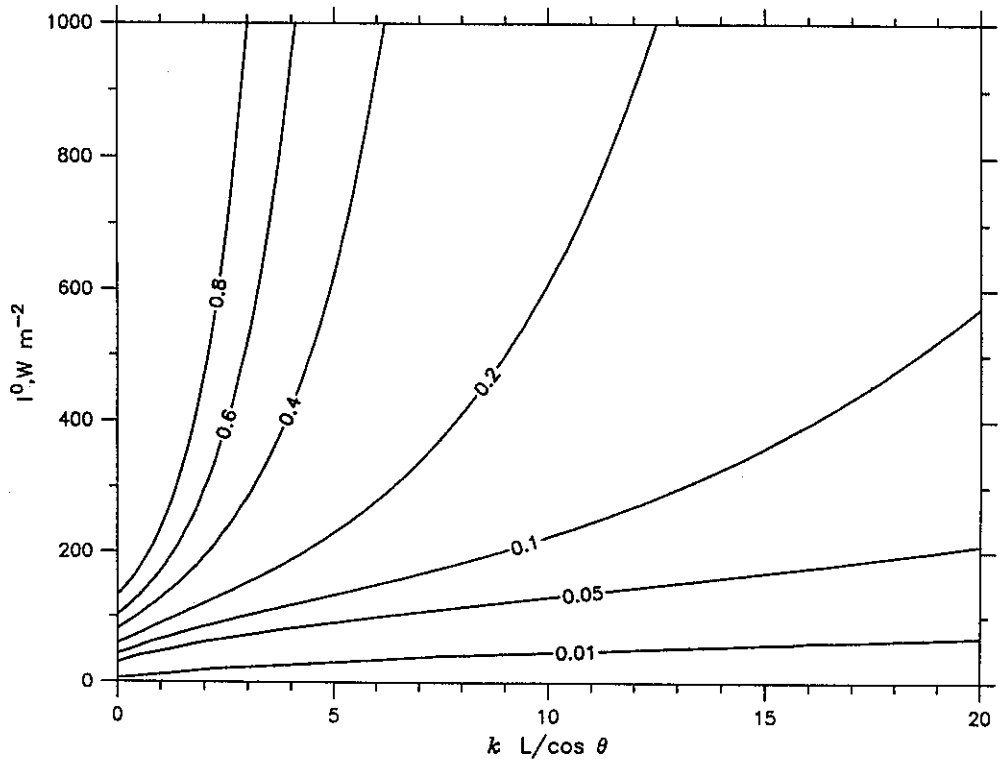

Fig. B1. Light correction factor ω for isoprene emission from a vegetation canopy (equation (B5)), as a function of the solar radiation incident at canopy top (I^0) and the canopy optical path ($kL/\cos\theta$).

APPENDIX C: COMPUTATION OF PLUME BOX AREAS

The area A_1 of box U1 includes the total urban area A_U occupied by 1/6°x1/4° urban cells in the 4°x5° grid square, plus the 4-hour fetch downwind of A_U:

$$A_1 = A_U + \max[\, \gamma A_U \, (\frac{W\Delta t}{w_U} - 1) \, , \, 0 \,] \qquad \text{(C1)}$$

Here γ is a correction factor accounting for overlap between plume boxes ($0 < \gamma \leq 1$), W is the mean wind speed in the mixed layer, Δt = 4 hours is the model time step, and w_U is the characteristic size of a city in the grid square. The value of w_U is defined by the largest cluster of contiguous urban cells and ranges from 20 to 80 km [*Sillman et al.*, 1990].

The area A_2 of box U2 is defined as the fraction f_U of the old box U1 advected downwind of the urban area over the past 4 hours, with rural air entrained into the plume by cross-flow diffusion:

$$A_2 = \gamma f_U A_1^o \, E \qquad \text{(C2)}$$

with

$$f_U = 1 - \frac{\max(w_U - W\Delta t, \, 0)}{\max(W_o \Delta t, \, w_U)} \qquad \text{(C3)}$$

$$E = \frac{[w_U^2 + 8K_y\Delta t]^{1/2}}{w_U} \qquad \text{(C4)}$$

Here A_1^o is the area of the old box U1, computed at the previous time step from equation (C1); W_o is the wind speed at the previous time step; E is an entrainment factor for rural air into the plumes [*Sillman et al.*, 1990]; and $K_y = 1\text{x}10^4$ m^2 s^{-1} is a cross-flow horizontal turbulent diffusion coefficient [*Gifford*, 1982]. The value of f_U is unity except under stagnant conditions ($W\Delta t < w_U$) when urban emissions may remain over cities for more than 4 hours.

The areas A_3 and A_4 of boxes P1 and P2 are computed with equations similar to (C1) and (C2), replacing A_U and w_U with their power plant analogs A_P and w_P. The area A_R of the rural box is obtained by difference:

$$A_R = A_T - \sum_{i=1}^{4} A_i \qquad \text{(C5)}$$

where A_T is the total area of the 4°x5° grid square.

The plume overlap correction factor γ is obtained by assuming that plumes advected downwind of urban or power plant cells are distributed randomly within the grid box. The total area A occupied by these plumes is

$$A = \sum_{i=1}^{4} A_i - A_U - A_P \qquad \text{(C6)}$$

Let A^* be the area occupied by these plumes in the absence of plume overlap (A^* is readily calculated using $\gamma = 1$ in equations (C1) and (C2)). We have $\gamma = A/A^*$ by definition. We can relate A and A^* by the differential equation

$$dA = (1 - \frac{A + A_U + A_P}{A_T}) \, dA^* \qquad \text{(C7)}$$

Integration of (C7) then yields

$$\gamma = \frac{(A_T - A_U - A_P)(1 - e^{-A^*/A_T})}{A^*} \qquad \text{(C8)}$$

APPENDIX D: CUMULATIVE PROBABILITY DISTRIBUTIONS

The cumulative probability distribution of concentrations at a rural site in the model is constructed by considering that the site may be located at any time step either in the rural box (i=1) or in one of the aged plume boxes U2 and P2 (i=2,3), with a probability p_i defined by the relative area A_i of each box:

$$p_i = \frac{A_i}{\sum_1^3 A_i} \quad \text{(D1)}$$

We assume that the rural site cannot be located in the fresh plume boxes U1 or P1 by definition of its rural character. For a time series of n 4-hour periods j=1, ..., n we retrieve a record (C_{ij}, p_{ij}) of concentrations at the site with corresponding probabilities, and derive the vector of ranked concentrations C_k (k=1,...3n) defined by $C_k \geq C_{k-1}$. The corresponding vector of integral probabilities ρ_k defines the cumulative probability distribution:

$$\rho_k = \frac{\sum_{k'=1}^{k} p_{k'}}{n} \quad \text{(D2)}$$

Acknowledgements. We thank our colleagues Y. J. Balkanski, M. Chin, E.W. Gottlieb, P.A. Spiro, and J.H. Yatteau for assistance in various aspects of this work and A.L. Lefohn for providing his analysis of AIRS data. We are indebted to S.J. Oltmans, D.D. Parrish, and J.R. Roberts for kindly communicating their data prior to publication. The paper was significantly improved by discussions with B.F. Farrell, S.J. Oltmans, D.H. Stedman, A.L. Torres, and M. Trainer and by comments from two reviewers. Support was provided by the Coordinating Research Council (Project AP-9), the Environmental Protection Agency (EPA-R814535-01-0), the National Aeronautics and Space Administration (NASA-NAGW-1230), the National Science Foundation (NSF-ATM-88-58074 and NSF-ATM-89-21119), and the Packard Foundation.

REFERENCES

Altshuller, A. P., Association of oxidant episodes with warm stagnating anticyclones, *J. Air Pollut. Control Assoc., 28*, 152-155, 1978.

Aneja, V.P., S. Businger, Z. Li, C.S. Claiborn, and A. Murthy, Ozone climatology at high elevations in the Southern Appalachians, *J. Geophys. Res., 96*, 1007-1021, 1991.

Barnes, R.A., A.R. Bandy, and A.L. Torres, Electrochemical concentration cell ozonesonde accuracy and precision, *J. Geophys. Res., 90*, 7881-7887, 1985.

Buhr, M. P., D. D. Parrish, R. B. Norton, F. C. Fehsenfeld, R. E. Sievers, and J. M. Roberts, Contribution of organic nitrates to the total reactive nitrogen budget at a rural eastern U.S. site, *J. Geophys. Res., 95*, 9809-9816, 1990.

Carmichael, G.R., L.K. Peters, and R.D. Saylor, The STEM-III regional scale acid deposition and photochemical oxidant model, I, An overview of model development and applications, *Atmos. Environ., 25(A)*, 2077-2090, 1991.

Chang, J.S., R.A. Brost, I.S.A. Isaksen, S. Madronich, P. Middleton, W.R. Stockwell, and C.J. Walcek, A three-dimensional Eulerian acid deposition model: Physical concepts and formulation, *J. Geophys. Res., 92*, 14,681-14.698, 1987.

Crutzen, P.J., The role of NO and NO_2 in the chemistry of the troposphere and stratosphere, *Ann. Rev. Earth Planet. Sci.*, 7, 443-472, 1979.

Decker, C.E., L.A. Ripperton, J.J.B. Worth, F.M. Vukovich, W.D. Bach, J.B. Tommerdahl, F. Smith, and D.E. Waggoner, Formation and transport of oxidants along the Gulf coast and in northern U.S., *EPA Rep., EPA-45013-76-003*, Environ. Protect. Agency, Research Triangle Park, N.C., 1976.

Environmental Protection Agency (EPA), The 1985 NAPAP emission inventory (version 2): development of the annual data and modeler's tapes, *EPA Rep., EPA-600/7-89-012a*, Research Triangle Park, N.C., 1989.

Environmental Protection Agency (EPA), National air pollutant emission estimates 1940-1990, *EPA Rep., EPA-450/4-91-026*, Environ. Protect. Agency, Research Triangle Park, N.C., 1991.

Evans, G.F., The national air pollution background network: final project report. *Rep. EPA 600/4-85-038*, Environmental Protection Agency, Research Triangle Park, NC, 1985.

Gifford, F.A., Horizontal diffusion in the atmosphere: A Lagrangian-dynamical theory, *Atmos. Environ.*, 16, 505-512, 1982.

Goldstein, A.H., J.W. Munger, B.C. Daube, M.L. Goulden, and S.C. Wofsy, Isoprene fluxes in a New England forest: A whole-system study (abstract), *EOS Trans. AGU, 73*,, (43), Fall Meeting Suppl., 76, 1992.

Guenther, A., P. Zimmerman, and M. Wildermuth, Natural volatile organic compound emission rate estimates for U.S. woodland landscapes, *Atmos. Environ.*, in press, 1993.

Hansen, J., G. Russell, D. Rind, P. Stone, A. Lacis, S. Lebedeff, R. Ruedy, and L. Travis, Efficient three-dimensional global models for climate studies: Models I and II, *Mon. Weather. Rev., 111*, 609-662, 1983.

Harman, J.R., Mean monthly North American anticyclone frequencies, 1950-79, *Mon. Weather. Rev., 115*, 2840-2848, 1987.

Hastie, D.R., P.B. Shepson, S. Sharma, and H.I. Schiff, The influence of the nocturnal boundary layer on secondary trace species in the atmosphere at Dorset, Ontario, *Atmos. Environ., 27(A)*, 533-541, 1993.

Hilsenrath, E., and 13 others, results from the balloon ozone intercomparison campaign (BOIC), *J. Geophys. Res., 91*, 13,137-13,152, 1986.

Jacob, D.J., and M.J. Prather, Radon-222 as a test of convection in a general circulation model, *Tellus, 42*, 118-134, 1990.

Jacob, D. J., S. Sillman, J. A. Logan, and S. C. Wofsy, Least independent variables method for simulation of tropospheric ozone, *J. Geophys. Res., 94*, 8497-8510, 1989.

Jacob, D.J., J.A. Logan, G.M. Gardner, R.M. Yevich, C.M. Spivakovsky, S.C. Wofsy, S. Sillman, and M.J. Prather, Factors regulating ozone over the United States and its export to the global atmosphere, *J. Geophys. Res.*, this issue.

Lamb, B., A. Guenther, D. Gay and H. Westberg, A national inventory of biogenic hydrocarbon emissions, *Atmos. Environ., 21*, 1695-1706, 1987.

Lawson, D.R., P.J. Groblicki, D.H. Stedman, G.A. Bishop, and P.L. Guenther, Emissions from in-use motor vehicles in Los Angeles: a pilot study of remote sensing and the inspection and maintenance program, *J. Air Waste Manage. Assoc., 40*, 1096-1105, 1990.

Lefohn, A.S., and V.A. Mohnen, The characterization of ozone, sulfur dioxide, and nitrogen dioxide for selected monitoring sites in the Federal Republic of Germany, *J. Air Pollut. Control Assoc., 36*, 1329-1337, 1986.

Lefohn, A.S., S.V. Krupa, and D. Wistanley, Surface ozone exposures measured at clean locations around the world, *Environ. Pollut., 63*, 189-224, 1990.

Lieth, H., Primary productivity of the major vegetation units of the world, in *Primary Productivity of the Biosphere*, pp. 203-216, edited by H. Lieth and R.H. Whittaker, Springer-Verlag, New York, 1975.

Lin, X., M. Trainer, and S.C. Liu, On the nonlinearity of tropospheric ozone production, *J. Geophys. Res.*, 93, 15,879-15,888, 1988.

Liu, M.-K., R.E. Morris, and J.P. Killus, Development of a regional oxidant model and application to the northeastern United States, *Atmos. Environ., 18*, 1145-1161, 1984.

Liu, S.C., M. Trainer, F.C. Fehsenfeld, D.D. Parrish, E.J. Williams, D.W. Fahey, G. Hubler, and P.C. Murphy, Ozone production in the rural troposphere and the implications for regional and global ozone distributions, *J. Geophys. Res., 92*, 4191-4207, 1987.

Logan, J.A., Nitrogen oxides in the troposphere: Global and regional budgets, *J. Geophys. Res., 88*, 10,785-10,807, 1983.

Logan, J.A., Tropospheric ozone: Seasonal behavior, trends and anthropogenic influence. *J. Geophys. Res., 90*, 10,463-10,482, 1985.

Logan, J. A., Ozone in rural areas of the United States, *J. Geophys. Res.*, *94*, 8511-8532, 1989.

Logan, J.A., M.J. Prather, S.C. Wofsy, and M.B. McElroy, Tropospheric chemistry: A global perspective, *J. Geophys. Res.*, *86*, 7210-7254, 1981.

Lurmann, F.W., A.C. Lloyd, and R. Atkinson, A chemical mechanism for use in long-range transport/acid deposition computer modeling, *J. Geophys. Res.*, 91, 10,905-10,936, 1986.

MacGregor, L., and H. Westberg, The effect of NMOC and ozone aloft on modeled urban ozone production and control strategies, *J. Air Waste Manage. Assoc.*, *40*, 1372-1377, 1990.

Matthews, E., Global vegetation and land use: new high-resolution data bases for climate studies, *J. Clim. Appl. Meteorol.*, 22, 474-487, 1983.

McKeen, S.A., E.-Y. Hsie, M. Trainer, R. Tallamraju, and S.C. Liu, A regional model study of the ozone budget in the eastern United States, *J. Geophys. Res.*, *96*, 10,809-10,845, 1991.

Mount, G.H., and F.L. Eisele, An intercomparison of tropospheric OH measurements at Fritz Peak Observatory, Colorado, *Science*, *256*, 1187-1190, 1992.

Mueller, P.K., and G.M. Hidy, The sulfate regional experiment: report of findings, *Rep. EA-1901 (3 volumes)*, Electr. Power Res. Inst., Palo Alto, Calif., 1983.

National Oceanic and Atmospheric Administration (NOAA), *Climatological Data - National Summary - Annual Summary*, vol. 29, National Climate Center, Asheville, North Carolina, 1978.

National Oceanic and Atmospheric Administration (NOAA), *Climatological Data - National Summary - Annual Summary*, vol. 30, National Climate Center, Asheville, North Carolina, 1979.

National Research Council (NRC), *Rethinking the Ozone Problem in Urban and Regional Air Pollution*, National Academy Press, Washington, D.C., 1991.

Oltmans, S.J., W.D. Kohmyr, P.R. Franchois, and W.A. Matthews, Tropospheric ozone: Variations from surface and ECC ozonesonde observations, in *Proceedings of the 1988 Quadrennial Ozone Symposium*, edited by R.D. Bojkov and P. Fabian, A. Deepak, Hampton, Va., 1989.

Parrish, D.D., et al., Systematic variations in the concentration of NO_x (NO plus NO_2) at Niwot Ridge, Colorado, *J. Geophys. Res.*, *95*, 1817-1836, 1990.

Parrish, D.D., M. Trainer, M.P. Buhr, B.A. Watkins, and F.C. Fehsenfeld, Carbon monoxide concentrations and their relation to concentrations of total reactive oxidized nitrogen at two rural U.S. sites, *J. Geophys. Res.*, *96*, 9309-9320, 1991.

Parrish, D.D., et al., The total reactive oxidized nitrogen levels and the partitioning between the individual species at six rural sites in eastern North America, *J. Geophys. Res.*, *98*, 2927-2939, 1993.

Perner, D., U. Platt, M. Trainer, G. Hubler, J. Drummond, W. Junkermann, J. Rudolph, B. Schubert, A. Volz and D.H. Ehhalt, Measurements of tropospheric OH concentrations: A comparison of field data with model predictions, *J. Atmos. Chem.*, *5*, 185-216, 1987.

Pierson, W.R., A.W. Gertler, and R.L. Bradow, Comparison of the SCAQS tunnel study with other on-road vehicle emission data, *J. Air Waste Manage. Assoc.*, *40*, 1495-1504, 1990.

Poulida, O., R.R. Dickerson, B.G. Doddridge, J.Z. Holland, R.G. Wardell, and J.G. Watkins, Trace gas concentrations and meteorology in rural Virginia, 1, Ozone and carbon monoxide, *J. Geophys. Res.*, *96*, 22461-22475, 1991.

Prather, M.J., Numerical advection by conservation of second-order moments, *J. Geophys. Res.*, *91*, 6671-6681, 1986.

Prather, M.J., M.B. McElroy, S.C. Wofsy, G. Russell, and D. Rind, Chemistry of the global troposphere: Fluorocarbons as tracers of air motion, *J. Geophys. Res.*, *92*, 6579-6613, 1987.

Rasmussen, R. A. and M. A. K. Khalil, Isoprene over the Amazon Basin, *J. Geophys. Res.*, *93*, 1417-1421, 1988.

Ridley, B.A., S. Madronich, R.B. Chatfield, J.G. Welega, R.E. Shetter, M.A. Carroll and D.D. Montzka, Measurements and model simulations of the photostationary state during the Mauna Loa Observatory Photochemistry Experiment: Implications for radical concentrations and ozone production and loss rates, *J. Geophys. Res.*, *97*, 10,375-10,388, 1992.

Roselle, S.J., T.E. Pierce, and K.L. Schere, The sensitivity of regional ozone modeling to biogenic hydrocarbons, *J. Geophys. Res.*, *96*, 7371-7394, 1991.

Rudolph, J., B. Vierkorn-Rudolph, and F.X. Meixner, Large-scale distribution of peroxyacetylnitrate: Results from the STRATOZ III flights, *J. Geophys. Res.*, *92*, 6653-6661, 1987.

Samson, P.J., and B. Shi, A meteorological investigation of high ozone values in American cities, report prepared for The United States Congress, Office of Technology Assessment, Washington, D.C., August, 1988.

Seinfeld, J.H., *Atmospheric Chemistry and Physics of Air Pollution*, p. 594, John Wiley, New York, 1986.

Sexton, K., and H. Westberg, Nonmethane hydrocarbon composition of urban and rural atmospheres, *Atmos. Environ.*, *18*, 1125-1132, 1984.

Shepson, P.B., J.W. Bottenheim, D.R. Hastie, and A. Venkatram, Determination of the relative ozone and PAN deposition velocities at night, *Geophys. Res. Lett.*, *19*, 1121-1124, 1992.

Sillman, S., Models for regional-scale production of ozone, Ph.D. thesis, Harvard Univ., Cambridge, Mass., 1988.

Sillman, S., J.A. Logan, and S.C. Wofsy, A regional scale model for ozone in the United States with subgrid representation of urban and power plant plumes, *J. Geophys. Res.*, *95*, 5731-5748, 1990.

Singh, H.B., Reactive nitrogen in the troposphere, *Environ. Sci. Technol.*, *21*, 320-327, 1987.

Spivakovsky, C.M., R. Yevich, J.A. Logan, S.C. Wofsy, M.B. McElroy, and M.J. Prather, Tropospheric OH in a three-dimensional chemical tracer model: An assessment based on observations of CH_3CCl_3, *J. Geophys. Res.*, *95*, 18,441-18,472, 1990*a*.

Spivakovsky, C.M., S.C. Wofsy, and M.J. Prather, A numerical method for parameterization of atmospheric chemistry: Computation of tropospheric OH, *J. Geophys. Res.*, *95*, 18,433-18,440, 1990*b*.

Tingey, D.T., M. Manning. L.C. Grothaus, and W.F. Burns, The influence of light and temperature on isoprene emission rates from live oak, *Physiol. Plant.*, *47*, 112-118, 1979.

Trainer, M., E. Y. Hsie, S. A. McKeen, R. Tallamraju, D. D. Parish, F. C. Fehsenfeld, and S. C. Liu, Impact of natural hydrocarbons on hydroxyl and peroxy radicals at a remote site, *J. Geophys. Res.*, *92*, 11,879-11,894, 1987.

Trainer, M., et al., Observations and modeling of the reactive nitrogen photochemistry at a rural site, *J. Geophys. Res.*, *96*, 3045-3063, 1991.

Tuazon, E.C., and R. Atkinson, A product study of the gas-phase reaction of methylvinylketone with the OH radical in the presence of NO_x, *Int. J. Chem. Kinet.*, *22*, 1141-1152, 1989.

Tuazon, E.C., and R. Atkinson, A product study of the gas-phase reaction of isoprene with the OH radical in the presence of NO_x, *Int. J. Chem. Kinet.*, *22*, 1221-1236, 1990*a*.

Tuazon, E.C., and R. Atkinson, A product study of the gas-phase reaction of methacrolein with the OH radical in the presence of NO_x, *Int. J. Chem. Kinet.*, *22*, 591-602, 1990*b*.

United Nations (UN), *1982 Energy Statistics Yearbook*, United Nations, New York, 1984.

Van Valin, C.C., M. Luria, J.D. Ray, and J.F. Boatman, A comparison of surface and airborne trace gas measurements at a rural Pennsylvania site, *J. Geophys. Res.*, *96*, 20,745-20,754, 1991.

Vaughan, W.W., M. Chan, B. Cantrell, and F. Pooler, A study of persistent elevated pollution episodes in the United States, *Bull. Am. Meteorol. Soc.*, *63*, 258-266, 1982.

Verstraete, M.M., Radiation transfer in plant canopies: Transmission of direct solar radiation and the role of leaf orientation, *J. Geophys. Res.*, *92*, 10,985-10,995, 1987.

Vukovich, F.M., and J. Fishman, The climatology of summertime O_3 and SO_2 (1977-1981), *Atmos. Environ.*, *20*, 2423-2433, 1986.

Wesely, M.L., Parameterization of surface resistance to gaseous dry deposition in regional-scale numerical models, *Atmos. Environ.*, *23*, 1293-1304, 1989.

Wesely, M.L., and B.B. Hicks, Some factors that affect the deposition rates of sulfur dioxide and similar gases on vegetation, *J. Air Pollut. Control Assoc.*, 27, 1110-1116, 1977.

Wolff, G.T., and P.J. Lioy, Development of an ozone river associated with synoptic scale episodes in the eastern United States, *Environ. Sci. Technol.*, *14*, 1257-1261, 1980.

G. M. Gardner, D. J. Jacob, J. L. Logan, J. W. Munger, C. M. Spivakovsky, S. C. Wofsy, and R. M. Yevich, Division of Applied Sciences and Department of Earth and Planetary Sciences, Pierce Hall, 29 Oxford Street, Harvard University, Cambridge, MA 02138.

M. Prather, Department of Earth Sciences, University of California, Irvine, CA 91272.

M. O. Rodgers, Department of Atmospheric Sciences, Georgia Institute of Technology, Atlanta, GA 30332.

S. Sillman, Department of Atmospheric, Oceanic and Space Sciences, University of Michigan, Ann Arbor, MI 48109.

H. Westberg, Department of Civil and Environmental Engineering, Washington State University, Pullman, WA 99164.

P. R. Zimmerman, National Center for Atmospheric Research, Boulder, CO 80307.

(Received July 13, 1992;
revised May 5, 1993;
accepted May 6, 1993.)